**A novel motif in calcimembrin/C16orf74 dictates multimeric dephosphorylation by calcineurin**

Devin A. Bradburn[1,7], Joana C. Reis[2,3,7], Shariq Qayyum[2,4,5], Thibault Viennet[2,3,6], Haribabu Arthanari[2,3], Martha S. Cyert[1]*

1. Department of Biology, Stanford University, Stanford, CA 94305, USA
2. Department of Cancer Biology, Dana-Farber Cancer Institute, Boston, Massachusetts, USA.
3. Department of Biological Chemistry and Molecular Pharmacology, Harvard Medical School, Boston, Massachusetts, USA.
4. Men's Health: Aging & Metabolism, Brigham and Women's Hospital, Harvard Medical School, Boston, MA, USA.
5. Cardiovascular Research Center, Department of Medicine, Massachusetts General Hospital and Harvard Medical School, Boston, MA, USA
6. Department of Chemistry and iNANO, Aarhus University, Aarhus, Denmark
7. Contributed equally to this work

*Corresponding author:
Department of Biology
410B Bass Biology Building
Stanford University
Stanford, CA 94305-5020
phone: 650 723-9970
fax: 650 724-9945
E-mail: mcyert@stanford.edu

**Abstract:**

Calcineurin, the $Ca^{2+}$/calmodulin-activated protein phosphatase, recognizes substrates and regulators via short linear motifs, PxIxIT and LxVP, which dock to distinct sites on calcineurin and determine calcineurin distribution and catalysis, respectively. Calcimembrin/C16orf74 (CLMB), an intrinsically disordered microprotein whose expression correlates with poor cancer outcomes, targets calcineurin to membranes where it may promote oncogenesis by shaping calcineurin signaling. We show that CLMB associates with membranes via lipidation, i.e. N-myristoylation and reversible S-acylation. Furthermore, CLMB contains an unusual composite 'LxVPxIxIT' motif, that binds the PxIxIT-docking site on calcineurin with extraordinarily high affinity when phosphorylated, $^{33}$LxVPxIxITxx(p)T$^{44}$. Calcineurin dephosphorylates CLMB to decrease this affinity, but Thr44 is protected from dephosphorylation when PxIxIT-bound. We propose that CLMB is dephosphorylated in multimeric complexes, where one PxIxIT-bound CLMB recruits calcineurin to membranes, allowing a second CLMB to engage via its LxVP motif to be dephosphorylated. *In vivo* and *in vitro* data, including nuclear magnetic resonance (NMR) analyses of CLMB-calcineurin complexes, supports this model. Thus, the CLMB composite motif imposes unique properties to calcineurin signaling at membranes including sensitivity to CLMB:calcineurin ratios, CLMB phosphorylation and dynamic S-acylation.

## Introduction

Calcium ($Ca^{2+}$) ions are spatially and temporally controlled in cells to regulate a wide array of biological processes (*1*). $Ca^{2+}$ signaling frequently occurs within membrane-associated microdomains that contain both effector proteins and their substrates. Thus, subcellular localization of calcineurin, the only $Ca^{2+}$-calmodulin (CaM) regulated serine/threonine protein phosphatase, dictates its signaling specificity(*2*). Calcineurin (CNA/B) is an obligate heterodimer composed of catalytic (CNA) and regulatory (CNB) subunits that is activated when $Ca^{2+}$/calmodulin binding relieves autoinhibition carried out by the CNA C-terminal domain. Calcineurin interacts with partners via two short linear motifs (SLiMs), LxVP and PxIxIT, which cooperate to promote dephosphorylation. PxIxIT binds to CNA independent of $Ca^{2+}$and anchors

calcineurin to substrates and regulators. In contrast, LxVP binds to a site composed of residues in both CNA and CNB and orients substrates for dephosphorylation at a separate catalytic site, marked by $Zn^{2+}$ and $Fe^{2+}$ ions (*3*). LxVP binding occurs only after activation by $Ca^{2+}$/CaM and is blocked by autoinhibitory sequences in CNA as well as the immunosuppressant drugs, Cyclosporin A and FK506 (*4, 5*).

Systematic discovery of PxIxIT and LxVP SLiMs has significantly expanded our knowledge of calcineurin signaling (*6-9*) and surprisingly identified at least 31 human proteins that harbor composite calcineurin-binding motifs containing contiguous LxVP and PxIxIT sequences that share a proline (LxVPxIxIT)(*9*). Although each SLiM in a composite motif can bind to its cognate site, they are unlikely to do so simultaneously, as their docking surfaces are ~60 Å apart on calcineurin. Thus, how or if these motifs promote dephosphorylation is unclear.

Here we elucidate how C16orf74, a short unstructured protein associated with poor outcomes in melanoma, pancreatic and head and neck cancer, is regulated by calcineurin via a composite motif (*10, 11*). We name C16orf74 calcimembrin (CLMB), because it associates with membranes via lipidation (N-myristoylation and S-acylation) and recruits calcineurin to these sites. CLMB is phosphorylated at Thr 44 (pThr44), and binds calcineurin with exceptionally high affinity because the flanking LxVP and pThr44 features (LxVPxIxITxx(p)T) enhance PxIxT-mediated binding to CNA. Calcineurin also dephosphorylates pThr44. but this residue is protected when CLMB is bound to the PxIxT-docking surface. Thus, we propose that dephosphorylation occurs in multimers, with one CNA/B bound to two CLMB molecules at the PxIxIT and LxVP-docking sites, respectively. NMR confirms formation of these complexes *in vitro*. Furthermore, this multimeric model predicts that CLMB dephosphorylation is sensitive to the relative levels of CLMB to calcineurin, which we demonstrate through in cell analyses and kinetic modeling of dephosphorylation *in vitro*. In summary, this work reveals how CLMB can dynamically shape calcineurin signaling through a mechanism dictated by its composite motif and reversible association with membranes.

## Results

**Calcimembrin is myristoylated and S-acylated.** CLMB lacks predicted transmembrane domains but may associate with membranes via lipidation (Figure 1A) (*10*). CLMB contains a glycine at position 2 (Gly2), a site frequently modified by myristate, a 14-carbon lipid whose co-translational addition can promote protein association with membranes (*12*). CLMB also has two cysteines near in its N-terminus, Cys7 and Cys14, one of which, Cys7, is predicted to be modified by S-acylation, the reversible addition of a fatty acid, usually a 16-carbon palmitate, that regulates membrane localization (*13*). To determine if CLMB is lipidated, we metabolically labeled HEK293 Flp-In T-REx cells inducibly expressing wildtype CLMB-FLAG ($CLMB_{WT}$) with YnMyr and 17-ODYA, alkyne-containing analogs of myristate and palmitate respectively (*14*). Following immunoprecipitation, analog incorporation was detected via addition of biotin using CLICK-chemistry followed by visualization with streptavidin (Figure 1B). $CLMB_{WT}$ incorporated YnMyr and 17-ODYA, indicating that the protein is both myristoylated and palmitoylated. To identify which residues were lipidated, we mutated proposed sites of S-acylation ($CLMB_{C7,14S}$), and myristoylation ($CLMB_{G2A}$ (Figure 1B). The mutants were expressed at low levels suggesting instability, which we countered by including a proteasome inhibitor (MG132) in the analyses. $CLMB_{C7,14S}$ showed no 17-ODYA incorporation but maintained YnMyr suggesting that Cys7 and/or Cys14 are S-acylated. By contrast, neither lipid modification was detected for $CLMB_{G2A}$, which confirms that Gly2 is myristoylated.

To determine if CLMB-FLAG is dually S-acylated at Cys7 and Cys14, we used an acyl-PEG exchange assay (APE) in which S-acylated groups are cleaved using hydroxylamine ($NH_2OH$) and exchanged for a PEGylated molecule that increases protein mass by 5 kDa for each S-acylated residue(*15*) (Figure 1C). Two slower migrating bands were observed for $CLMB_{WT}$. $CLMB_{C7S}$ lacked the upper band, while $CLMB_{C7,14S}$ was unmodified, indicating that $CLMB_{WT}$ contains two S-acylated residues, i.e. Cys7 and Cys14. $CLMB_{G2A}$ also displayed two sites of S-acylation, suggesting that metabolic labeling (Figure 1B) was not sufficiently sensitive to detect these modifications. Together these findings establish that CLMB is myristoylated at Gly2 and S-acylated at Cys7 and Cys14.

**Dynamic S-acylation of CLMB mediates membrane association.** To examine whether CLMB-FLAG S-acylation is dynamic (*16*), we carried out a pair of pulse-chase analyses with two metabolic labels (Figure 1D and 1E). L-AHA, an azide-containing methionine analog detected CLMB-FLAG protein levels, while in parallel, 17-ODYA detected S-acylation. CLMB-FLAG was immunopurified (IP) after labeling for one hour followed by a 30-minute chase with DMSO or Palmostatin B (PalmB), a pan-inhibitor of thioesterases that remove S-acylation (*17*). Quantifying the 17-ODYA to L-AHA ratio revealed that incorporation of palmitate into CLMB increased ~3-fold when thioesterases were inhibited (PalmB vs DMSO). This indicates that S-acylation of CLMB turns over rapidly relative to its rate of degradation.

To determine if lipidation mediates CLMB membrane recruitment, we analyzed the localization of $CLMB_{WT}$ and lipidation defective mutants, $CLMB_{G2A}$ and $CLMB_{C7,14S}$. Detergent-assisted subcellular fractionation showed that $CLMB_{WT}$ was primarily membrane associated, while both mutants were predominantly cytosolic (Figure 1F and 1G). Therefore, N-myristoylation and dynamic S-acylation of CLMB stabilize the protein and mediate its association with membranes.

**The composite SLiM in CLMB mediates binding to and dephosphorylation by calcineurin.** Next, we examined how each part of CLMB's composite motif, LDVPDIIIT, contributes to calcineurin binding by generating mutants, $CLMB_{IxITMut}$ (LDVPD**AIAA**) and $CLMB_{LxVMut}$, (**A**D**A**PDIIIT) (Figure 1A) that disrupt each motif independently without altering the shared proline. To examine binding of these mutants to calcineurin, the association of CLMB-FLAG with GFP-tagged calcineurin (CNA-GFP complexed with endogenous CNB) was assessed following purification of calcineurin from lysates of HEK293 cells co-transfected with these constructs (Figure 2A and 2B). $CLMB_{WT}$ but not $CLMB_{IxITMut}$ co-purified with calcineurin, showing that this interaction was PxIxIT-dependent. Co-purification of $CLMB_{LxVMut}$ with calcineurin was somewhat reduced relative to $CLMB_{WT}$, indicating a smaller contribution to calcineurin binding. Furthermore, when expressed and analyzed by SDS-polyacrylamide gel electrophoresis (SDS-PAGE), both mutants displayed two electrophoretic forms, with a slower migrating form also faintly observed for $CLMB_{WT}$. These represent CLMB containing pThr44 and are absent in mutants lacking this

residue ($CLMB_{T44A}$, $CLMB_{T44A+LxVMut}$). These observations indicate that calcineurin binds to CLMB and dephosphorylates pT44, which is disrupted when either the LxVP or PxIxIT portion of the composite motif is compromised. Finally, we confirmed that pThr44 enhances binding to calcineurin, as the slower migrating forms of $CLMB_{WT}$ and $CLMB_{LxVMut}$ predominantly co-purified with calcineurin (*10*). Indeed, $CLMB_{T44A}$ displayed reduced binding to calcineurin, which was further reduced by mutating LxV ($CLMB_{T44A+LxVMut}$).

The contributions of PxIxIT, LxVP, and pThr44 to calcineurin binding were also examined by measuring the extent of CLMB co-localization with calcineurin (CNA-GFP complexed with endogenous CNB) via immunofluorescence (IF). When co-transfected into MCF7 cells $CLMB_{WT}$-FLAG recruits calcineurin to membranes (Figure 2C, 2D). In contrast, when co-expressed with $CLMB_{IxITMut}$ calcineurin is predominantly cytosolic. $CLMB_{LxVMut}$ and $CLMB_{T44A}$ also display reduced colocalization with calcineurin, mirroring the trends observed in co-purification analyses.

Finally, the ability of calcineurin to dephosphorylate pThr44 in CLMB was demonstrated *in vitro* using peptide substrates that encode residues 21-50 (Figure 1A and 2 E). The peptide from $pCLMB_{WT}$ but not $pCLMB_{LxVMut}$ was dephosphorylated showing that, as for other calcineurin substrates, the LxVP motif is required for catalysis (*18*). Together, these data show that both the LxVP and PxIxIT components of the composite motif are functional, that CLMB is a calcineurin substrate, and that pThr44 enhances CLMB binding to calcineurin.

**Phosphorylated Thr44 and the LxVP motif enhance CLMB binding to the PxIxIT docking site.** To quantitatively assess CLMB-calcineurin interaction, we used isothermal titration calorimetry (ITC) and fluorescence polarization anisotropy (FP) to measure binding of CLMB peptides containing the composite SLiM (residues 21-50) to purified, catalytically inactive CNA/B containing $CNA_{Trunc+H151Q}$. This mutant lacks the C-terminal autoinhibitory region of CNA, which allows LxVP motifs to bind to CNA/B in the absence of $Ca^{2+}$/CaM(*19*). ITC revealed that the phosphorylated $CLMB_{WT}$ peptide ($pCLMB_{WT}$) binds calcineurin at a one-to-one ratio with the highest reported affinity for any substrate, ($K_D$= 8.29 nM), (Figure

127 3A). FP using FITC-labelled peptides revealed that phosphorylation of Thr44 enhances CLMB binding to
128 calcineurin ~30-fold ($K_D$ = 12.29nM vs 384.5 nM) (Figure 3B). The concordance between measurements
129 made with a tag-free CLMB peptide (ITC) vs. a peptide tagged with fluorescein isothiocyanate (FITC) (FP)
130 (8.29 vs 12.29 nM for $pCLMB_{WT}$), shows that the tag does not significantly affect binding affinity. Given
131 the high-throughput capability of FP, this method was used for the remaining comparisons. To test if the
132 high affinity $pCLMB_{WT}$-calcineurin binding observed was PxIxIT-mediated, we used FP to assess the ability
133 of CLMB peptides to compete for calcineurin binding with FITC-PVIVIT, a well characterized PxIxIT
134 peptide(*20, 21*) (Figure 3C). $pCLMB_{WT}$ competed with PVIVIT most effectively, (Figure 3C, 3E) with
135 peptides lacking the LxVP motif ($pCLMB_{LxVMut}$), or pThr44 ($CLMB_{WT}$) showing reduced competition.
136 $pCLMB_{IxITMut}$ lacking the PxIxIT motif was unable to displace PVIVIT from CNA/B. When these
137 experiments were repeated using FITC-$pCLMB_{WT}$ peptide in place of PVIVIT (Figure 3D, 3E), a similar
138 pattern was observed, although the absence of pThr44 showed a much greater (~30x) reduction in $K_i$.
139 Importantly, full length CLMB protein displayed a near equal ability to displace FITC-$pCLMB_{WT}$, showing
140 that CLMB peptides accurately mimic full length CLMB binding to calcineurin (Figure S1A and S1B).
141 Altogether, these data show that, like PVIVIT, $pCLMB_{WT}$ peptides bind to the PxIxIT docking groove on
142 CNA and that flanking residues, i.e. LxV and pThr44, enhance binding to form an extended
143 LxVPxIxITxxT(p) sequence with exceptionally high affinity for calcineurin.

144 **NMR analysis shows CLMB binding to two sites on calcineurin.** Next, to investigate the structure of
145 CLMB in the presence and absence of calcineurin, we used solution-state NMR. 88% of non-proline
146 backbone resonances were assigned using a standard set of triple-resonance experiments, utilizing full-
147 length dually $^{13}C$- and $^{15}N$-labeled CLMB (76 residues) that was expressed in *E.coli* (Figure 4A and S2A).
148 To assess CLMB secondary structure, we employed Talos-N, a computational method that predicts
149 backbone torsion angles from NMR chemical shifts. This revealed that CLMB is disordered overall, but
150 contains two regions that displayed a tendency to form a β-strands (Figure S2B): Residues I38-I40 include
151 the PxIxIT, consistent with binding of this motif-type to CNA as a β-strand (*4, 22*). N-terminal residues,

Q12-V15, were also predisposed to localized folding suggesting possible involvement in other binding interactions.

To map the interaction interface of calcineurin on CLMB, we focused first on PxIxIT-mediated interactions by titrating $^{15}$N-labeled CLMB with varying molar ratios of monomeric recombinant CNA in the absence of CNB and monitoring the interaction through $^{15}$N-$^{1}$H SOFAST-HMQC experiments. CNA can bind to PxIxIT motifs but lacks the LxVP binding surface found at the interface of CNA and CNB(*4*). Due to the size of the CLMB-CNA complex, we anticipated significant broadening of NMR signals at the interaction interface. This broadening can also arise from the exchange kinetics between the observable CLMB and the titrant, CNA, making it challenging to distinguish the two effects. As expected, at a molar ratio of 2:1 (CLMB: CNA), many of the CLMB signals undergo significant line broadening, which become more pronounced at a molar ratio to 1:1, due to the majority of CLMB being bound to CNA. This is particularly the case for signals corresponding to the PxIxIT and LxVP motifs, indicating, as observed in FP experiments, that LxV residues participate in binding to the PxIxIT interface (Figure 4B and C, Figure S2C). Line broadening across the majority of CLMB residues indicates that the interaction interface on CLMB extends beyond the PxIxIT and LxVP motifs (Figure 4B and C). Interactions with the N- and C-terminal residues of CLMB may be an avidity-driven effect, anchored by PxIxIT binding, as has been reported for other calcineurin substrates (*23*).

To investigate binding that may occur at the LxVP docking site of calcineurin, we next titrated CLMB with the heterodimeric CNA/B complex. Signal broadening at the N-terminus of CLMB was more pronounced with CNA/B relative to CNA alone, suggesting possible interactions between CLMB and CNB (Figure 4B, C vs 4D, E, and S2D). These include the Q9-V12 region that displayed partial folding in the absence of calcineurin. At a molar ratio of 2:1 (CLMB: CNA/B), more broadening is observed in LxVP but not PxIxIT residues when compared to the interaction with CNA (Figure 4B vs 4D, and S2C). However, at a molar ratio of 1:1, where essentially all CLMB should be PxIxIT-bound (given the higher $K_D$ for PxIxIT vs LxVP and our working concentrations), the pattern of line broadening at the composite motif is similar when

complexed with either CNA or CNA/B (Figure 4C vs 4E). Together these findings show that when in excess (2 CLMB: 1 CNA/B), CLMB engages calcineurin (CNA/B) through both its LxVP and PxIxIT motifs. To investigate these interactions further, we carried out structural predictions for 2 CLMB molecules and CNA/B using AlphaFold 3(*24*). Consistent with our NMR analyses, the models show two copies of CLMB simultaneously bound to CNA/B, one each at the LxVP and PxIxIT docking sites. Predicted binding for CLMB containing pThr44 to CNA/B was nearly identical, however with the LxVP-bound CLMB showing an additional interaction of pThr44 with the active site as would occur during catalysis (Figure S3A-S3C). Thus, these models suggest that formation of multimeric complexes (2 CLMB: 1 CNA/B) will facilitate dephosphorylation.

**Calcineurin dephosphorylates CLMB by forming multimers.** Next, we sought to determine if, as predicted, dephosphorylation of pT44 is promoted when CLMB is in excess (2 CLMB: 1 CNA/B) but is inhibited by lower CLMB: CNA/B ratios which favor formation of PxIxIT-bound complexes that protect pThr44 from dephosphorylation. To this end, we inducibly expressed $CLMB_{WT}$-FLAG in HEK293 Flp-In T-REx cells and examined its phosphorylation status in cells where calcineurin is expressed at endogenous levels or overexpressed (i.e. transfected with GFP-CNA, which complexes with endogenous CNB). In stark contrast to its behavior with typical substrates, overexpression of calcineurin caused CLMB-FLAG phosphorylation to increase (Figure 5A, B, and S4A). Intact PxIxIT binding rather than catalytic activity was required for this effect, as overexpressing calcineurin that is catalytically inactive (containing GFP-$CNA_{H151Q}$), but not calcineurin that is defective for PxIxIT binding (containing GFP-$CNA_{NIR}$), increased CLMB-FLAG phosphorylation (Figure S4B)(*25*). We predicted that further increasing CLMB expression in these calcineurin overexpressing cells would increase the CLMB:CNA/B ratio, leading to greater dephosphorylation of CLMB-FLAG. Thus, we overexpressed V5-tagged CLMB in HEK293 Flp-In T-REx cells inducibly expressing CLMB-FLAG with overexpressed calcineurin (GFP-CNA complexed with endogenous CNB). As predicted, the amount of phosphorylated $CLMB_{WT}$-FLAG observed was reduced by introducing additional $CLMB_{WT}$-V5 (Figure 5A-C). This effect was dependent on PxIxIT binding, as

introducing $CLMB_{IxITMut}$-V5 did not decrease $CLMB_{WT}$-FLAG phosphorylation, but $CLMB_{LxVMut}$-V5, which contains an intact PxIxIT motif, did. We repeated these experiments using $CLMB_{IxITMut}$-FLAG, which is partially phosphorylated regardless of calcineurin levels. Surprisingly, $CLMB_{IxITMut}$-FLAG was predominantly dephosphorylated when co-expressed with $CLMB_{WT}$-V5 or $CLMB_{LxVMut}$-V5 but not $CLMB_{IxITMut}$-V5 (Figure 5A and B). Thus, although the LxVP and PxIxIT components of the CLMB composite motif are both required for efficient dephosphorylation, they do not need to be on the same molecule. A single copy of CLMB must have an LxVP to mediate its own dephosphorylation but can utilize the PxIxIT of neighboring copies to recruit calcineurin, promote LxVP binding, and be dephosphorylated (Figure 5C).

To demonstrate more precisely how the ratio of CLMB to calcineurin affects dephosphorylation, we conducted a series of *in vitro* dephosphorylation assays using a fixed substrate concentration (100nM $pCLMB_{WT}$ or $pCLMB_{IxITMut}$ peptides) with varied concentrations of purified calcineurin (CNA/B) (20nM, 100nM and 200nM). For $pCLMB_{IxITMut,}$ dephosphorylation rate increased with the calcineurin concentration. However, $pCLMB_{WT}$ showed no change under these same conditions (Figure 5D). We propose that this unusual result reflects competition between the two different modes of pCLMB binding to calcineurin: high affinity binding to the PxIxIT-docking site, which prevents T44 dephosphorylation, vs low affinity binding to the LxVP-docking site which promotes dephosphorylation. With a substrate that contains only an LxVP motif (i.e. $pCLMB_{IxITMut}$), increasing calcineurin concentration accelerates substrate binding to the LxVP docking site and dephosphorylation. However, with a substrate that contains a composite motif (i.e. $pCLMB_{WT}$), this increased LxVP-mediated binding is offset by an equivalent reduction in the amount of pCLMB that is available to be dephosphorylated due to substrate binding via the PxIxIT docking site and pThr44 protection. We used kinetic modeling to assess how well this proposed mechanism explains the observed dynamics of $pCLMB_{WT}$ and $pCLMB_{IxITMut}$ dephosphorylation (Figure S5A and B). When simultaneously fitting results with both substrates, the kinetic model showed remarkable

agreement with the data and estimated rate constants that approach values reported in the literature (Figure 5D and S5C)(*6, 18*). Together, these analyses provide evidence that the phosphorylated composite motif in CLMB imposes unique attributes on its dephosphorylation. In addition to a requirement for $Ca^{2+}$ and CaM, the presence of this composite motif dictates that substrate must be in excess of calcineurin so that multimeric complexes can form and carry out dephosphorylation.

**Discussion**

In this study, we reveal how a composite LxVPxIxITxx(p)T motif functions in calcineurin binding and dephosphorylation. For engaging calcineurin (CNA/B), we can break down the thermodynamic contributions of the motif in CLMB into three parts: (i) the core PxIxIT motif, (ii) pThr44, and (iii) the LxVP motif. Our FP analyses reveal that the PxIxIT motif provides the largest contribution to the binding free energy, as mutating this motif ($pCLMB_{IxITMut}$) decreased binding by more than two orders of magnitude. Phosphorylation acts as the second major driver of binding affinity, imparting a ~30-fold increase in binding affinity, from $K_D$ ~400nM to 13 nM for the non-phosphorylated versus phosphorylated peptide (Figure 3). Similarly, phosphorylation at this position was reported to enhance the affinity of the PxIxIT motif in Cabin1, a calcineurin regulator that like CLMB, contains a PxIxIT followed by "PP(p)TP"(*26, 27*). In contrast, mutating the LxVP motif only modestly reduces affinity for calcineurin (~5X), indicating a smaller role in binding. These data suggest that the PxIxIT motif primarily anchors the peptide, while phosphorylation significantly enhances the overall affinity.

Using full length recombinant CLMB, NMR studies reveal that the binding interface for calcineurin extends beyond the composite motif, with notable involvement of the N-terminal residues in interactions. However, this interaction may differ in a cellular environment, where the N-terminus is anchored to the membrane via N-myristoylation and S-acylation. At higher molar ratios of CLMB to calcineurin (CNA/B), NMR data suggest that a second CLMB molecule binds, by utilizing the LxVP motif to bind its cognate stie at the

252 CNA/B heterodimeric interface. These findings are supported by *in vivo* data, showing that increasing
253 calcineurin expression enhanced levels of phosphorylated CLMB, which then decreased when CLMB
254 expression was further increased.

255 Based on all our data, we present two models for how CLMB may shape calcineurin activity *in vivo* (Figure
256 6). Dynamic S-acylation promotes CLMB association with membranes (Figure 6A, Step 1), where, when
257 phosphorylated, it recruits a localized pool of calcineurin via high affinity PxIxIT-mediated binding (Figure
258 6A, Step 2). In the presence of a $Ca^{2+}$ signal, $Ca^{2+}$ and CaM activate calcineurin which exposes the LxVP
259 docking site(*28*). If CLMB is in excess relative to calcineurin and PxIxIT binding is fully saturated, a
260 second CLMB molecule will bind via its LxVP motif which positions pThr44 for dephosphorylation at the
261 active site (Figure 6A, Step 3). As the population of CLMB shifts to the dephosphorylated form, decreased
262 PxIxIT binding affinity (Figure 3) promotes calcineurin dissociation from CLMB, allowing the enzyme to
263 engage and dephosphorylate other nearby LxVP- and PxIxIT-containing substrates (Figure 6A, Step 4). A
264 similar requirement for 'low' PxIxIT affinity was demonstrated for the another signaling scaffold, AKAP5,
265 which binds and concentrates both calcineurin and NFAT near L-type $Ca^{2+}$ channels in neurons to promote
266 NFAT dephosphorylation. In that case, increasing the affinity of the native PxIxIT in AKAP5 for calcineurin
267 ~two-fold significantly impaired NFAT activation due to increased sequestering of calcineurin(*29*).

268 In our second model (Figure 6B), active calcineurin-pCLMB dimers (1 CLMB: 1 CNA/B) directly engage
269 and dephosphorylate substrates at the membrane that contain only an LxVP motif (Figure 6B, step 3). Many
270 candidate calcineurin substrates are predicted to contain only an LxVP, but if and how the majority are
271 dephosphorylated by calcineurin has yet to be uncovered. The best characterized example is the cAMP-
272 dependent protein kinase type II-alpha regulatory subunit (PRKAR2A), which depends on the PxIxIT motif
273 within its binding partner, the AKAP5 scaffold, to recruit calcineurin for its dephosphorylation(*9, 30*). In
274 our second model (Figure 6B), active calcineurin-pCLMB dimers (1 CLMB: 1 CNA/B) directly engage
275 and dephosphorylate such PxIxIT-less substrates at the membrane (Figure 6B, step 3). Simply recruiting
276 calcineurin to membranes, where association kinetics are 20-30 fold faster than in the cytosol of eukaryotic

cells, may enhance LxVP binding causing their efficient dephosphorylation despite lacking their own PxIxIT motif(*31*). Such division of the PxIxIT and LxVP motifs among two molecules may also allow for the extremely high affinity PxIxIT observed in CLMB. In substrates that contain both LxVP and PxIxIT motifs, stable PxIxIT binding may limit enzymatic efficiency by slowing product release. However, acting only as a scaffold, CLMB can remain tightly associated with calcineurin via PxIxIT-binding while other substrates cycle in and out of the LxVP-binding surface and are dephosphorylated. In this scenario (Figure 6B), calcineurin remains at the membrane either until CLMB levels increase sufficiently to allow CLMB dephosphorylation and calcineurin dissociation (Figure 6B step 4) or until CLMB is de-acylated. In both models, intracellular $Ca^{2+}$ dynamics, CLMB protein levels, and S-acylation/de-acylation activities combine to modulate calcineurin signaling. Future studies aim to identify the palmitoyl acyltransferases (PATs) and acyl protein thioesterases (APTs) that dynamically regulate CLMB S-acylation to better understand how these critical regulators contribute to calcineurin-CLMB signaling *in vivo*.

Another missing player in our model is the kinase(s) that phosphorylates CLMB. One candidate is the stress-activated p38 mitogen-activated protein kinase (MAPK), which phosphorylates the PP(p)TP site in Cabin1 and is predicted to phosphorylate Thr44 of CLMB (*32*). Because phosphorylation increases CLMB-calcineurin affinity, kinase activation is required to prime regulation of calcineurin signaling by CLMB. However, phosphorylation also establishes a negative feedback mechanism, with dephosphorylation decreasing calcineurin's interaction with its substrate. Thus, regulators that modify kinase activity may also significantly affect CLMB-calcineurin signaling dynamics.

Because the sequence in CLMB is the first composite motif to be analyzed, further studies are needed to establish whether dephosphorylation via multimeric complexes is a general property of such motifs. Several predicted LxVPxIxIT motifs do occur in ion channels, such as TRPM6, that assemble into higher order complexes(*9, 33*). One possibility is that such composite motifs, which are present in at least thirty additional human proteins, may in some cases provide a safety mechanism, by ensuring that calcineurin dephosphorylates only multimeric substrates(*9*).

302 The major challenge that lies ahead is to identify the molecular targets and physiological functions that are
303 regulated by calcineurin-CLMB. CLMB increases proliferation and migration of some pancreatic ductal
304 adenocarcinoma (PDAC) derived cell lines, suggesting that CLMB shapes calcineurin signaling to promote
305 oncogenesis(*10*). Indeed, high CLMB expression is associated with poor patient outcomes for PDAC,
306 melanoma and head and neck cancer(*10, 11*). Mechanisms underlying these activities have not yet been
307 identified, but these cancers may provide good starting points for examining how CLMB modifies
308 calcineurin signaling in a biologically and clinically relevant context(*34*).
309
310 **Materials and Methods**
311
312 **Cell culture and transfection:**
313 Cells were cultured at 37 °C in 5% $CO_2$. HEK293 Flp-In TReX and MCF7 cell lines were grown in standard
314 media containing Dulbecco's modified eagle's medium (DMEM) with 4.5 mg/mL glucose, L-glutamine,
315 and sodium pyruvate (Cytiva SH30243.FS) supplemented with 10% fetal bovine serum (Corning
316 MT35010CV). Transfections were done according to manufacturer instructions. HEK293 cells were
317 transfected using lipofectamine 2000 (Thermo Fisher Scientific 11668019). MCF7 cells were transfected
318 using Transfex ATCC transfection reagent (ATCC ACS-4005).
319
320 **Stable cell line generation:**
321 On day one, 9.6 x $10^5$ HEK293 Flp-In TReX cells were transfected using lipofectamine 2000 with 1.5 µg
322 pOG44 and 0. 5 µg pcDNA5 FRT TO encoding proteins of interest in a 6 well dish (plasmid # 2801, 2852,
323 2860, 2861, 2862, 2863, 2864, and 2880). Transfections were done according to manufacturer instructions.
324 On day two, transfected cells were passaged onto 10cm plates. On day three, selection was started using
325 media containing 3 µg blasticidin and 200 ng/mL hygromycin. Selection media was replaced every 2-3
326 days until distinct colonies appeared. Colonies were selected using cloning rings and expanded before being
327 stored in liquid nitrogen.

**Metabolic labeling to detect CLMB lipidation:**

HEK293 Flp-In TReX lines stably expressing $CLMB_{WT}$, $CLMB_{C7,14S}$, or $CLMB_{G2A}$ were induced with 10 ng/mL doxycycline for 24 hours and split evenly among three 10 cm tissue culture dishes. The following day, cells were rinsed with PBS and incubated in DMEM containing 4.5 mg/mL glucose, L-glutamine, sodium pyruvate, 2% FBS, and either 20 µM YnMyr (Click Chemistry Tools 1164-5), 30 µM 17-ODYA (Cayman Chemical Company 34450-18-5), or vehicle (ethanol and DMSO) overnight. Cells were then co-incubated with 20 µM YnMyr, 30 µM 17-ODYA, or vehicle and 20 µM MG132 (EMD Millipore 474787-10MG) for 4 hours before washed twice in PBS and frozen at -80 °C. Cells were lysed in 400 µL TEA lysis buffer (50 mM TEA pH 7.4, 150 mM NaCl, 1% triton X-100, and 1 mM PMSF) by inverting for 15 minutes at 4 °C. Lysates were passed five times through a 27-gauge needle, centrifuged at 16,000 x *g* for 15 minutes at 4 °C and protein content determined by Pierce BCA protein assay kit (Thermo Fisher Scientific 23225). 25 µg total lysate was removed as input and 0.5 mg total protein was incubated with pre-washed magnetic M2 anti-FLAG (Sigma-Aldrich M8823-5ML) beads at 4 °C for 1.5 hours while inverting. Beads were washed 3X with modified RIPA (50 mM TEA pH 7.4, 150 mM NaCl, 1% Triton X-100, 0.1% SDS, and 1% sodium deoxycholate) and resuspended in 40 µL 1x PBS. 10 µL of 5x click reaction mix (1x PBS, 0.5 mM biotin azide, 5 mM TCEP, 0.5 mM TBTA, 5 mM $CuSO_4$) was added and reactions incubated for 1 hour at 24 °C, shaking at 550 RPM. Beads were washed 3X in modified RIPA and eluted 2X using 30 µL of 1 mg/mL FLAG peptide in modified RIPA buffer. 12 µL of non-reducing 6x SDS sample buffer was added to eluate before heating at 95 °C for 2 minutes and analysis by SDS-PAGE. Note that addition of reducing agents to SDS sample buffer results in loss of 17-ODYA signal. Samples were transferred to nitrocellulose membrane and lipidation was detected using fluorophore-tagged streptavidin, and total CLMB with anti-FLAG. Immunoblots were imaged using a Licor Odyssey CLx and quantified with Image Studio software.

**Metabolic pulse-chase labeling assay to assess dynamic CLMB S-acylation:**

353 HEK293 Flp-In TReX cells stably expressing $CLMB_{WT}$-FLAG were induced with 10 ng/mL doxycycline
354 for 48 hours. Cells were rinsed 2X in PBS and incubated in methionine free DMEM supplemented with 5%
355 charcoal-stripped FBS, 1 mM L-glutamate, 1 mM sodium pyruvate, 0.4 mM cysteine and 10 ng/mL
356 doxycycline along with vehicle (ethanol), 30 µM 17-ODYA, 50 µM L-AHA, or 17-ODYA and L-AHA
357 together. After two hours, cells were washed 2X in PBS and either harvested immediately or incubated in
358 standard media supplemented with 10 µM palmitic acid and 10 ng/mL doxycycline, with or without 10 µM
359 palmostatin B (EMD Millipore 178501-5MG). Cells were rinsed in PBS and frozen at -80 °C. Metabolic
360 labeling was done as described in the previous section with the exception that two rounds of labeling were
361 done. First, Cy5-azide (Click Chemistry Tools AZ118-1) was linked to 17-ODYA. Then, cells were washed
362 and L-AHA was linked to AF-488 (Click Chemistry Tools 1277-1) alkyne before being washed three
363 additional times and eluted using FLAG peptide. Samples were resolved via SDS-PAGE and in-gel
364 fluorescence was read using the GE Amersham Typhoon imaging system. Images were quantified in Image
365 Studio. The proportion of S-acylated CLMB is calculated as Cy5/A-488 normalized to the no chase control.
366

367 **Acyl-PEG exchange:**

368 HEK293 Flp-In TReX lines stably expressing $CLMB_{WT}$, $CLMB_{C7S}$, $CLMB_{C7,14S}$, or $CLMB_{G2A}$ were induced
369 with 10 ng/mL doxycycline for 48 hours. Cells were rinsed 2X in PBS and stored at -80 °C. Cells were
370 lysed in 400 µL lysis buffer (50 mM TEA pH 7.3, 150 mM NaCl, 2.5% SDS, 1 mM PMSF, 100 units
371 benzonase) at 37 °C for 20 minutes, shaking at 800 RPM. Lysates were passed 10X through a 27-gauge
372 needle, centrifuged at 16,000 x *g* for 5 minutes and protein quantified by BCA. Lysates were adjusted to 2
373 mg/mL and incubated with 10 mM TCEP for 30 minutes at room temperature. Cysteines were protected by
374 incubating with 25 mM NEM for 2 hours at 40 °C, shaking at 800RPM. Protein was precipitated over night
375 with four volumes of acetone at -20 °C, centrifuged at 16,000 x *g* for 20 minutes at 4 °C and washed 4X in
376 70% acetone. Acetone was removed, pellets air-dried to remove all traces of acetone and resuspended in 75
377 µL Buffer A (50 mM TEA pH 7.3, 150 mM NaCl, 4% SDS, 0.2% triton X-100, 4 mM EDTA) for 1 hour at
378 40 °C, shaking at 800 RPM. Samples were centrifuged at 16,000 x *g* for 2 minutes, 7 µL removed as input,

379 and the remainder split into +cleavage and -cleavage fractions. The +cleavage sample containing 1% SDS
380 was treated with 750 μM hydroxylamine (final concentration) for 1 hour at 30 °C, rotating end over end.
381 Following methanol-chloroform precipitation (ice cold, final concentrations 42% methanol, 16%
382 chloroform) samples were centrifuged at 16,000 x *g* for 20 minutes at 4 °C, aqueous layer removed, washed
383 3X with 100% methanol and air dried. Pellets were resuspended as described in Buffer A and incubated in
384 1 mM mPEG-Mal (Methoxypolyethylene glycol maleimide, 5 kDa, 63187 Sigma-Aldrich) for 2 hours at
385 room temp, rotating end over end. Samples were methanol-chloroform precipitated as described,
386 resuspended in Lysis buffer with 1X SDS-PAGE sample buffer, resolved using SDS-PAGE and visualized
387 via immunoblotting with mouse anti-FLAG to detect CLMB-FLAG. Endogenous calnexin was detected
388 using anti-calnexin antibodies. Immunoblots were imaged using a Licor Odyssey CLx and quantified with
389 Image Studio software.
390
391 **Detergent-assisted subcellular fractionation:**
392 HEK293 Flp-In TReX lines stably expressing $CLMB_{WT}$, $CLMB_{C7,14S}$, or $CLMB_{G2A}$ were induced with 10
393 ng/mL doxycycline for 48 hours and 20 μM MG132 (EDM Millipore 474787-10MG) for 4 hours prior to
394 harvesting. Cells were washed 2X in PBS, harvested and immediately lysed in 600 μL of Cytoplasm Buffer
395 (10 mM HEPES pH 6.8, 100 mM NaCl, 300 mM sucrose, 3 mM $MgCl_2$, 5 mM EDTA, 0.015% digitonin,
396 1x halt protease inhibitor cocktail (Thermo Fischer scientific 78442)) at 4 °C for 15 minutes. 60 μL of total
397 lysate was removed as input and the remainder centrifuged at 1000 x *g* for 10 min at 4 °C. The supernatant
398 was removed as cytoplasmic fraction and the pellet washed 2X in PBS and resuspended in 600 μL
399 membrane buffer (10 mM HEPES pH 7.5, 100 mM NaCl, 300 mM sucrose, 3 mM $MgCl_2$, 3 mM EDTA,
400 0.5% Triton X-100, 1x halt protease inhibitor cocktail) for 30 minutes at 4 °C turning end over end.
401 Insoluble material was pelleted by centrifugation at 5000 x *g* for 10 minutes at 4 °C and supernatant
402 removed as membrane fraction. Both fractions were centrifuged at 12,000 x *g* at 4 °C for 10 minutes.
403 Samples were heated in 1X SDS sample buffer at 95 °C for 5 minutes, resolved via SDS-PAGE,
404 immunoblotted and CLMB-FLAG detected using anti-FLAG antibodies; anti-GM130 and anti-α-tubulin

were used as membrane and cytosolic markers respectively. Immunoblots were imaged using a Licor Odyssey CLx and quantified with Image Studio software. CLMB in cytosolic and membrane fractions were quantified as $CLMB_{Cyto}/(CLMB_{Cyto}+ CLMB_{Mem})$ and $CLMB_{Mem}/(CLMB_{Cyto} + CLMB_{Mem})$, respectively.

**Immunofluorescence, microscopy, and image analysis:**

MCF7 cells were co-transfected (as described previously) with equal amounts of pcDNA5 encoding $CLMB_{WT}$, $CLMB_{IxITMut}$, $CLMB_{LxVMut}$, $CLMB_{T44A}$ and pcDNA5 encoding CNA-GFP. The following day cells were plated on poly-lysine coated 12 mm, #1.5H glass coverslips (ThorLabs). On day three, cells were washed in PBS and fixed in 100% methanol for 10 minutes at -20 °C. Coverslips were washed 3 times in 1x PBS, blocked (1x PBS, 200 mM glycine, 2.5% FBS) for 30 minutes at room temperature, then incubated in primary antibody diluted in blocking buffer for 1 hour before being washed 3 times in 1x PBS and incubated for 1 hour in secondary antibody solution. Following three additional washes, coverslips were mounted using Prolong Glass mountant with NucBlue stain. After sitting overnight at room temperature, coverslips were imaged using a Lionheart FX automated widefield microscope with a 20X Plan Fluorite WD 6.6 NP 0.45 objective. For each coverslip, a 7 by 7 grid of non-overlapping images was automatically taken. All images were manually assessed and those with defects (debris, bubbles, out-of-focus, etc.) were filtered out. Images were analyzed using an automated pipeline using CellProfiler(*35*). Briefly, cells were identified by their nuclei and all those lacking CLMB-FLAG staining removed. CLMB-FLAG signal was used to define the cell body and all cells containing one or more fully saturated pixels in the CLMB-FLAG or CNA-GFP channels were removed. Pearson's correlation coefficient between CLMB-FLAG and CNA-GFP was determined for each individual cell. >500 cells per condition were analyzed.

**GFP-Trap coimmunoprecipitation:**

HEK293 cells were co-transfected (as described previously) with pcDNA5 encoding CNA-GFP and pcDNA5 encoding $CLMB_{WT}$, $CLMB_{IxITMut}$, $CLMB_{LxVMut}$, $CLMB_{T44A}$, or $CLMB_{LxVMut+T44A}$. 24 hours post-transfection, cells were washed 2X in PBS and frozen at -80 °C. Cells were lysed in 500 µL lysis buffer (50

431 mM Tris pH 7.5, 150 mM NaCl, 1% NP-40), aspirated 5X with a 27-gauge needle, centrifuged at 16,000 x
432 *g* for 20 min at 4 °C and protein quantified via BCA. 100 mg total protein was removed as input. Lysates
433 were adjusted to 0.5% NP-40 and 500 µg of protein incubated with pre-washed magnetic GFP-TRAP beads
434 (ChromoTek gtma-20) for 2 hours at 4 °C, turning end over end. Beads were magnetized, washed 3 times
435 and eluted with 50 µL of 2x SDS PAGE sample buffer. Samples were resolved via SDS-PAGE and
436 visualized via immunoblotting with anti-flag antibodies to detect CLMB-FLAG and anti-GFP to detect
437 CNA-GFP. Anti-GAPDH was used as a loading control for inputs. Immunoblots were imaged using a Licor
438 Odyssey CLx and CLMB-calcineurin binding was quantified with Image Studio software. Co-purified
439 CLMB was normalized using the following: ($CLMB_{IP}/CLMB_{Input}$)/GFP-$CNA_{IP}$. Additionally, all values are
440 displayed relative to $CLMB_{WT}$ which is set at 1.
441
442 **Protein expression and purification:**
443 CNA catalytic dead mutant H151Q with an N-terminal $His_6$-CNA (residues 1–391) and CNB (residues 1–
444 170) subunits were expressed using *E. coli* BL21(DE3) cells in Lysogeny Broth (LB) supplemented with
445 50 µg/mL ampicillin. Protein expression was induced with 1 mM isopropyl β-d-1-thiogalactopyranoside
446 (IPTG) at 18 °C. Cells were lysed using a Fisherbrand™ Model 505 Sonic Dismembrator and lysates were
447 centrifuged at 46,000 × *g* at 4 °C for 45 minutes. The protein was purified by incubation with nickel-
448 nitriloacetic acid (Ni-NTA) agarose resin (Qiagen) for 3h at 4 °C. The resin was washed with 50 mM Tris
449 pH 8.0, 250 mM NaCl, 20 mM imidazole, and 1 mM TCEP. A buffer containing 50 mM Tris pH 8.0, 250
450 mM NaCl, 300 mM imidazole, and 1 mM TCEP was used for elution. Calcineurin was further purified by
451 SEC (Superdex® 200 Increase 10/300 GL) using Phosphate-buffered saline (PBS) and $CaCl_2$ 1mM as the
452 final buffer.
453
454 **Fluorescence polarization binding assay:**
455 All FP measurements were performed on a multifunctional microplate reader (EnVision, Perkin Elmer) in
456 black 384-well microplates (Corning, Cat No 3575) with 30 µL of the assay solution per well. 480-nm

excitation and 535-nm emission filters were used for the FP measurements. In the FP saturation binding experiments, 5 nM FITC labeled peptides were mixed with increasing concentrations of calcineurin in PBS and 500 μM $CaCl_2$ buffer (from 0 to 25 μM). The FP values were plotted against the log of the protein concentrations, and the dissociation constant (apparent $K_D$) was obtained from the resulting sigmoidal curve as analyzed in GraphPad Prism 10.

**Flourescence polarization competition assay:**

For the competitive binding assay, a mixture containing 5 nM FITC-labeled CLMB peptides and CNA/B (0.08 and 2 μM for CLMB vs PVIVIT experiments) was incubated with serial dilutions of unlabeled peptides for 30 minutes at room temperature. The FP values were determined, and the $IC_{50}$ values, i.e., the concentrations required for 50% displacement of the FITC labeled peptide, were calculated in GraphPad Prism 10. The $K_i$ values of competitive inhibitors were calculated based on a previously reported method(*36*), further adapted by(*37*). Briefly, the relation of $K_i$ and $IC_{50}$ in competitive inhibition as applied to protein-ligand–inhibitor (P–L–I) interactions, can be summarized by the following equation:

$$K_i = \frac{IC_{50}}{(\frac{\mathrm{L}}{K_d} + 1)}$$

Where L stands for the concentration of ligand, i.e., the FITC-labeled peptide used in the FP binding assay; and $K_D$ corresponds to the dissociation constant of the same FITC-labeled peptide resulting from the performed FP binding assay.

**ITC measurements:**

Isothermal titration calorimetry (ITC) experiments were performed using an Affinity ITC from TA Instruments (New Castle, DE) equipped with an autosampler in a buffer containing 50 mM HEPES, pH 8.0, 150 mM NaCl, 1 mM TCEP, 500μM $CaCl_2$ at 25 °C. 40 μM protein solution in the calorimetric cell was titrated with 100 μM peptide solution using 0.5 μL injection in 200-sec intervals using stirring speed

at 125rpm. The resulting isotherm was fitted with a single site model to yield thermodynamic parameters of ΔH, ΔS, stoichiometry, and $K_D$ using NanoAnalyze software (TA instruments).

**NMR analyses:**

All NMR data were acquired using TopSpin3.4 (Bruker), processed with NMRPipe v.2020/2021 and analyzed with CCPNmr v3(*38, 39*). Structural biology applications were compiled by the SBGrid consortium. Three-dimensional (3D) NMR experiments were conducted on a Bruker spectrometer operating at 600 MHz, equipped with TCI cryoprobes and z-shielded gradients. Samples of approximately180-µM 2H-, $^{13}$C- and $^{15}$N-calcimembrin in 20 mM Hepes pH 6.9, 100 mM NaCl, 0.5 mM EDTA, 1 mM TCEP and 5% v/v $^{2}$H2O were used. Temperature was set to 25˚C. Chemical shift assignments are deposited in the Biological Magnetic Resonance Bank (BMRB) under accession code 52641.

The NMR titration samples were prepared by adding unlabeled calcineurin A/B complex or unlabeled calcineurin subunit A into solutions of U-[$^{15}$N]-labeled calcimembrin (50 µM) to reach a ratio of 0.5:1 (25 µM unlabeled calcineurin) or 1:1 (50 µM unlabeled calcineurin). Two-dimensional (2D) spectra were acquired using SOFAST-HMQC on a Bruker 800 MHz Avance III spectrometer equipped with a TXO cryoprobe and z-shielded gradients(*40*). Data was processed using NmrPipe and analyzed with CCPNmr. Secondary structure prediction was analyzed using Talos-N(*22*).

**AlphaFold 3 modeling:**

Calcineurin-CLMB complex modeling was done using AlphaFold 3 on AlphaFold server(*24*). Modeling was done using truncated $CNA_{1-491}$, CNB, and two copies of CLMB phosphorylated at Thr44. $Zn^{2+}$ and $Fe^{3+}$ (found in the calcineurin active site) and four $Ca^{2+}$ ions (bound to CNB) were included in modeling. All images were generated in UCSF ChimeraX 1.8(*41*).

***In vivo* analysis of CLMB phosphorylation status:**

506 HEK293 FLIP-In TreX cells stably expressing $CLMB_{WT}$-FLAG, $CLMB_{IxITMut}$-FLAG, $CLMB_{LxVMut}$-FLAG,
507 or $CLMB_{T44A}$-FLAG were transfected with empty vector or pcDNA5 FRT TO encoding CNA-GFP
508 alongside empty vector or pcDNA5 FRT TO encoding $CLMB_{WT}$-V5, $CLMB_{IxITMut}$-V5, or $CLMB_{LxVMut}$-V5.
509 Protein expression was induced for 24 hours with 10 ng/mL doxycycline, cells washed 2X in PBS and
510 stored at -80 °C. Cells were lysed (50 mM Tris pH 8, 150 mM NaCl, 1% NP-40, 0.1% SDS, 0.5% sodium
511 dodecyl sulfate, 1x Halt protease inhibitor cocktail) and resolved via SDS-PAGE and detected via
512 immunoblotting.
513
514 ***In vitro* CLMB phospho-peptide dephosphorylation:**
515 $CLMB_{WT}$, $CLMB_{IxITMut}$, and $CLMB_{LxVMut}$ phospho-peptides were synthesized by Vivitide, resuspended in
516 10 mM Tris pH 8.0 and dephosphorylated at 26 °C in reaction buffer (50 mM Tris pH 8.0, 100 mM NaCl,
517 6 mM $MgCl_2$, 2 mM $CaCl_2$, 1 mM EGTA, 0.1 mg/mL BSA, 1 mM DTT, 0.5 µM MDCC-PBP (Thermo
518 Scientific PV4406), 1 µM CaM (Millipore Sigma 208694-1MG)). Reactions were initiated by addition of
519 CLMB peptide to a final concentration of 200nM. Reactions took place in a total of 50 µL in a corning
520 black 96 well vessel and were monitored continuously via fluorescence emitted by phosphate bound
521 MDCC-PBP (EX:425/ EM:460). Phosphate standards were used to convert fluorescence intensity to
522 phosphate concentration. Data were analyzed using Prism software and the rate of phosphate production
523 was obtained by fitting data to a single exponential.
524
525 **Kinetic Modeling:**
526 Dephosphorylation data were fit by simulation and non-linear regression using Kintek Explorer™. Sigma
527 values for each individual replicate were obtained using the double exponential afit function. All replicates
528 were simultaneously fit to the models described in supplemental figures 2A and 2B. Curve offsets capped
529 at a maximum offset of 50nM. Substrate concentration was allowed to vary by 15% during fitting. Offsets
530 and substrate concentrations for each curve and fit quality metrics are displayed in Tables S1-S3. Final
531 graphs display averaged ($n \geq 5$) phosphate released at each timepoint with the corresponding fit.

**Statistical analysis:**

Statistical analysis was done using Graphpad Prism version 10.2.2. All data is displayed as representative images or mean values with standard deviation error bars unless otherwise noted. All data represent three independent experiments unless otherwise indicated in figure legends. Image analysis of CLMB-calcineurin colocalization was conducted using the following number of cells: $CLMB_{WT}$ = 525, $CLMB_{IxITMut}$ = 641, $CLMB_{LxVMut}$ = 500, $CLMB_{T44A}$ = 517. Statistical significance was calculated using one-way analysis of variance (ANOVA) with corrections for multiple comparisons as indicated.

**Data availability:**

All original scans of immunoblots, immunofluorescence images, and AlphaFold predictions can be accessed through Mendeley Data (to be made available upon publication). Plasmids and reagents will be shared upon request. NMR chemical shift assignments are deposited in the Biological Magnetic Resonance Bank (BMRB) under accession code 52641.

**Acknowledgements:**

We thank Norman Davey and members of the Cyert and Arthanari labs, in particular Angela Barth and Sneha Roy, for helpful discussion. We are grateful to Callie Wigington and Makena Pule for their early contributions to the project and to Rick Russell for feedback on the kinetic modeling. We thank Ilya Bezprozvanny for suggesting the name, calcimembrin.

**Funding:**

MSC and DAB are supported by NIH grant R35 GM136243. DAB also acknowledges support from NIH grant T32 GM007276. HA, JCR, SQ and TV acknowledge grant R01 GM136859 from NIH.

**Author Contributions:**

MSC, DAB, HA and JCR conceived the studies. SQ and TV provided early NMR analysis of CLMB-calcineurin complexes. DAB, supervised by MSC, carried out experiments and analyzed data for Figures 1, 2, and 5, and prepared figures. JCR, supervised by HA, carried out experiments and analyzed data for Figures 3 and 4. TV carried out secondary structure analyses. DAB and MSC wrote the manuscript in consultation with HA and JCR.

**References:**


1. M. D. Bootman, G. Bultynck, Fundamentals of Cellular Calcium Signaling: A Primer. *Cold Spring Harb Perspect Biol* **12**, (2020).
2. I. Ulengin-Talkish, M. S. Cyert, A cellular atlas of calcineurin signaling. *Biochim Biophys Acta Mol Cell Res* **1870**, 119366 (2023).
3. J. Aramburu, A. Rao, C. B. Klee, Calcineurin: from structure to function. *Curr Top Cell Regul* **36**, 237-295 (2000).
4. S. Grigoriu *et al.*, The molecular mechanism of substrate engagement and immunosuppressant inhibition of calcineurin. *PLoS biology* **11**, e1001492 (2013).
5. J. Roy, M. S. Cyert, Identifying New Substrates and Functions for an Old Enzyme: Calcineurin. *Cold Spring Harb Perspect Biol* **12**, (2020).
6. B. L. Brauer *et al.*, Leveraging New Definitions of the LxVP SLiM To Discover Novel Calcineurin Regulators and Substrates. *ACS Chem Biol* **14**, 2672-2682 (2019).
7. S. R. Sheftic, R. Page, W. Peti, Investigating the human Calcineurin Interaction Network using the piLxVP SLiM. *Scientific reports* **6**, 38920 (2016).
8. E. Tsekitsidou *et al.*, Calcineurin associates with centrosomes and regulates cilia length maintenance. *J Cell Sci* **136**, (2023).
9. C. P. Wigington *et al.*, Systematic Discovery of Short Linear Motifs Decodes Calcineurin Phosphatase Signaling. *Mol Cell* **79**, 342-358 e312 (2020).
10. T. Nakamura *et al.*, Overexpression of C16orf74 is involved in aggressive pancreatic cancers. *Oncotarget* **8**, 50460-50475 (2017).
11. M. Uhlen *et al.*, Towards a knowledge-based Human Protein Atlas. *Nat Biotechnol* **28**, 1248-1250 (2010).
12. T. Meinnel, C. Dian, C. Giglione, Myristoylation, an Ancient Protein Modification Mirroring Eukaryogenesis and Evolution. *Trends Biochem Sci* **45**, 619-632 (2020).
13. M. Blanc, F. P. A. David, F. G. van der Goot, SwissPalm 2: Protein S-Palmitoylation Database. *Methods Mol Biol* **2009**, 203-214 (2019).
14. M. C. Yap *et al.*, Rapid and selective detection of fatty acylated proteins using omega-alkynyl-fatty acids and click chemistry. *Journal of lipid research* **51**, 1566-1580 (2010).
15. A. Percher *et al.*, Mass-tag labeling reveals site-specific and endogenous levels of protein S-fatty acylation. *Proc Natl Acad Sci U S A* **113**, 4302-4307 (2016).
16. M. F.S. *et al.*, Mechanisms and functions of protein S-acylation. *Nat Rev Mol Cell Biol*, (2024).
17. F. J. Dekker *et al.*, Small-molecule inhibition of APT1 affects Ras localization and signaling. *Nat Chem Biol* **6**, 449-456 (2010).

18. D. K. Blumenthal, K. Takio, R. S. Hansen, E. G. Krebs, Dephosphorylation of cAMP-dependent protein kinase regulatory subunit (type II) by calmodulin-dependent protein phosphatase. Determinants of substrate specificity. *J Biol Chem* **261**, 8140-8145 (1986).
19. B. A. Perrino, L. Y. Ng, T. R. Soderling, Calcium regulation of calcineurin phosphatase activity by its B subunit and calmodulin. Role of the autoinhibitory domain. *J Biol Chem* **270**, 340-346 (1995).
20. J. Aramburu *et al.*, Affinity-driven peptide selection of an NFAT inhibitor more selective than cyclosporin A. *Science* **285**, 2129-2133 (1999).
21. H. Li, L. Zhang, A. Rao, S. C. Harrison, P. G. Hogan, Structure of calcineurin in complex with PVIVIT peptide: portrait of a low-affinity signalling interaction. *J Mol Biol* **369**, 1296-1306 (2007).
22. Y. Shen, A. Bax, Protein structural information derived from NMR chemical shift with the neural network program TALOS-N. *Methods Mol Biol* **1260**, 17-32 (2015).
23. R. Hendus-Altenburger *et al.*, Molecular basis for the binding and selective dephosphorylation of Na(+)/H(+) exchanger 1 by calcineurin. *Nat Commun* **10**, 3489 (2019).
24. J. Abramson *et al.*, Accurate structure prediction of biomolecular interactions with AlphaFold 3. *Nature* **630**, 493-500 (2024).
25. H. Li, A. Rao, P. G. Hogan, Structural delineation of the calcineurin-NFAT interaction and its parallels to PP1 targeting interactions. *J Mol Biol* **342**, 1659-1674 (2004).
26. S. Lee *et al.*, The optimized core peptide derived from CABIN1 efficiently inhibits calcineurin-mediated T-cell activation. *Exp Mol Med* **54**, 613-625 (2022).
27. H. Q. Nguyen *et al.*, Quantitative mapping of protein-peptide affinity landscapes using spectrally encoded beads. *Elife* **8**, (2019).
28. S. J. Li *et al.*, Cooperative autoinhibition and multi-level activation mechanisms of calcineurin. *Cell research* **26**, 336-349 (2016).
29. H. Li *et al.*, Balanced interactions of calcineurin with AKAP79 regulate Ca2+-calcineurin-NFAT signaling. *Nature structural & molecular biology* **19**, 337-345 (2012).
30. T. W. Church *et al.*, AKAP79 enables calcineurin to directly suppress protein kinase A activity. *Elife* **10**, (2021).
31. W. Y. C. Huang, S. G. Boxer, J. E. Ferrell, Jr., Membrane localization accelerates association under conditions relevant to cellular signaling. *Proc Natl Acad Sci U S A* **121**, e2319491121 (2024).
32. J. L. Johnson *et al.*, An atlas of substrate specificities for the human serine/threonine kinome. *Nature* **613**, 759-766 (2023).
33. C. H. Huang, Y. C. Chen, C. C. Chen, Physical interaction between calcineurin and Cav3.2 T-type Ca2+ channel modulates their functions. *FEBS Lett* **587**, 1723-1730 (2013).
34. A. S. Manalan, C. B. Klee, Activation of calcineurin by limited proteolysis. *Proc Natl Acad Sci U S A* **80**, 4291-4295 (1983).
35. D. R. Stirling *et al.*, CellProfiler 4: improvements in speed, utility and usability. *BMC Bioinformatics* **22**, 433 (2021).
36. Y. Cheng, W. H. Prusoff, Relationship between the inhibition constant (K1) and the concentration of inhibitor which causes 50 per cent inhibition (I50) of an enzymatic reaction. *Biochem Pharmacol* **22**, 3099-3108 (1973).

37. R. Z. Cer, U. Mudunuri, R. Stephens, F. J. Lebeda, IC50-to-Ki: a web-based tool for converting IC50 to Ki values for inhibitors of enzyme activity and ligand binding. *Nucleic acids research* **37**, W441-445 (2009).
38. F. Delaglio *et al.*, NMRPipe: a multidimensional spectral processing system based on UNIX pipes. *J Biomol NMR* **6**, 277-293 (1995).
39. W. F. Vranken *et al.*, The CCPN data model for NMR spectroscopy: development of a software pipeline. *Proteins* **59**, 687-696 (2005).
40. P. Schanda, E. Kupce, B. Brutscher, SOFAST-HMQC experiments for recording two-dimensional heteronuclear correlation spectra of proteins within a few seconds. *J Biomol NMR* **33**, 199-211 (2005).
41. E. C. Meng *et al.*, UCSF ChimeraX: Tools for structure building and analysis. *Protein Sci* **32**, e4792 (2023).

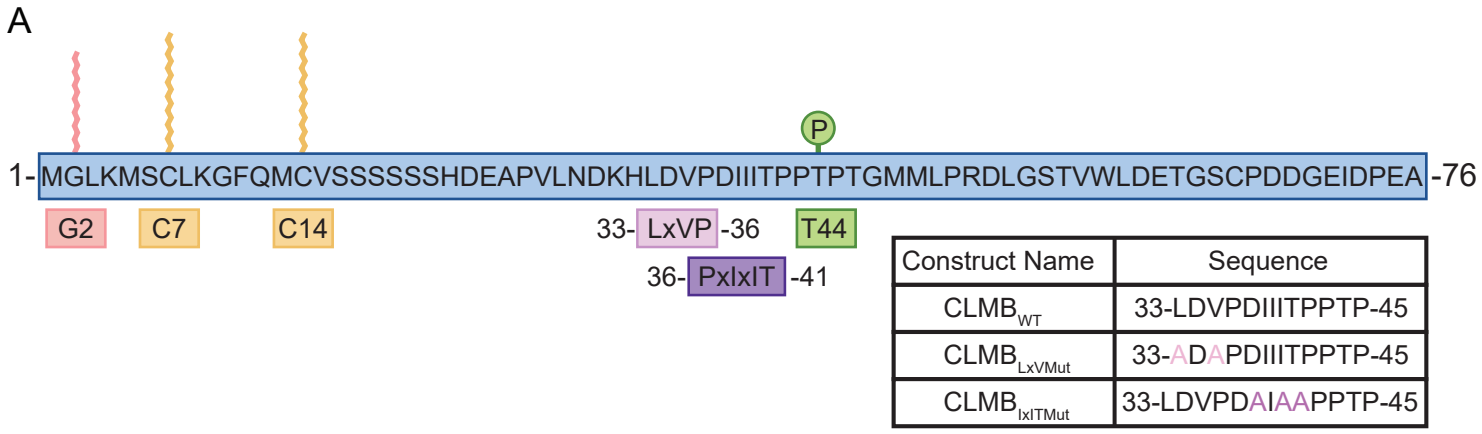


| Construct Name | Sequence |
|---|---|
| $CLMB_{WT}$ | 33-LDVPDIIITPPTP-45 |
| $CLMB_{LxVMut}$ | 33-ADAPDIIITPPTP-45 |
| $CLMB_{IxITMut}$ | 33-LDVPDAIAAPPTP-45 |

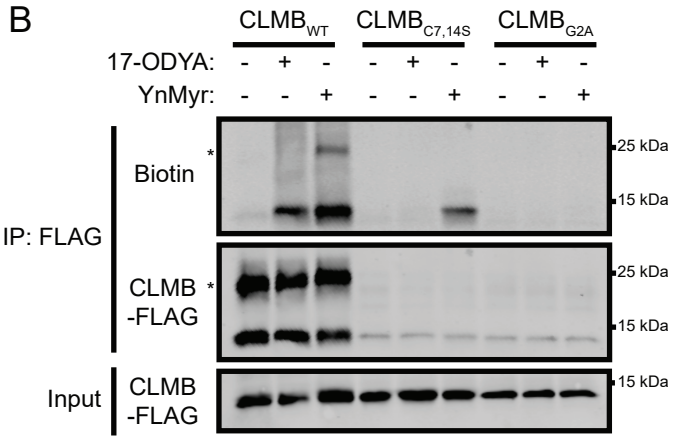


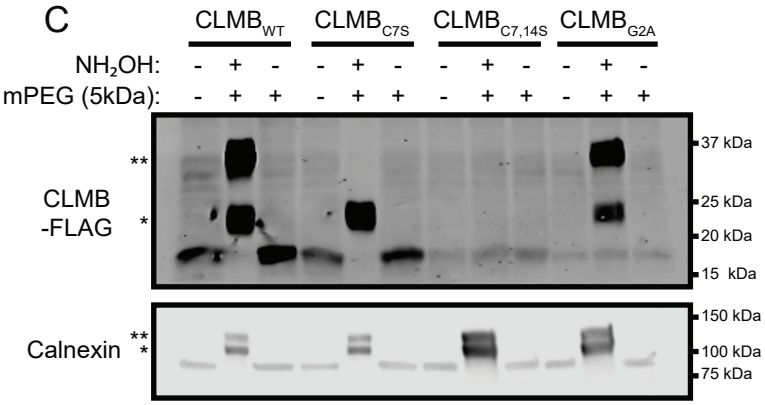


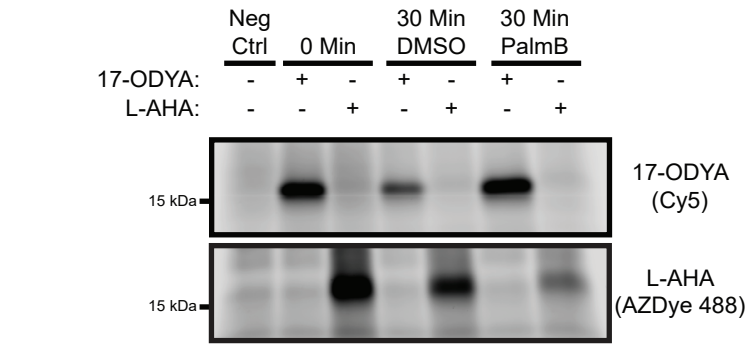


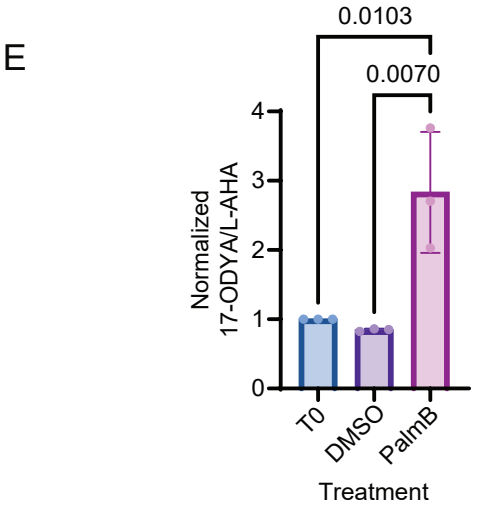


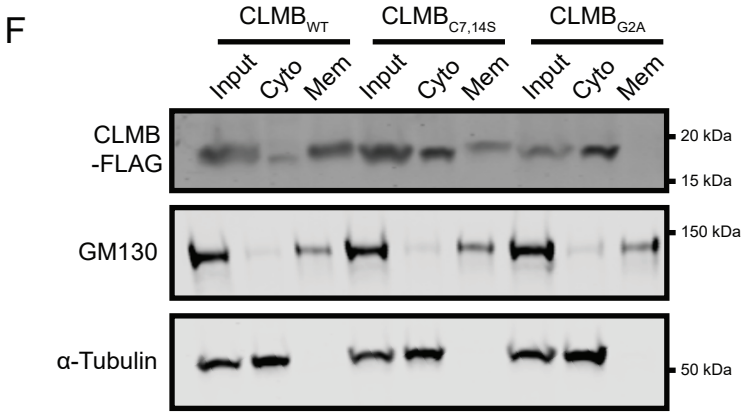


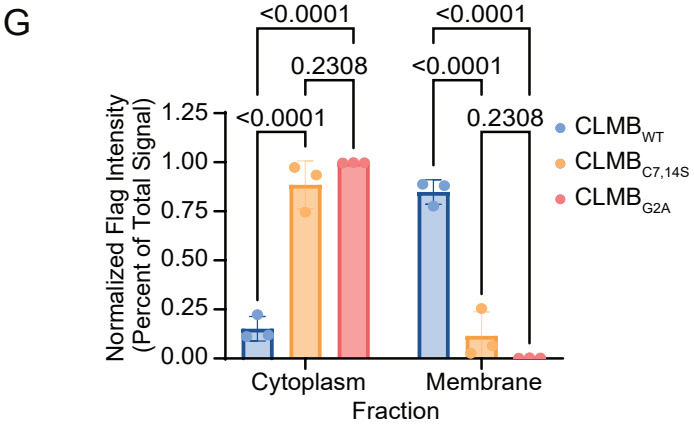

**Figure 1: Calcimembrin localizes to membranes via protein lipidation.**

**a** Schematic of CLMB. N-myristoylation (red); S-acylated cysteines (yellow); phospho-Thr44 (green); Calcineurin binding motifs LxVP (pink) and PxIxIT (purple). Mutant sequences are shown for $CLMB_{LxVMut}$ and $CLMB_{IxITMut}$.

**b** CLMB incorporates analogs of palmitate (17-ODYA) or myristate (YnMyr) as indicated. Cells were treated with 20 µM MG132 prior to harvesting. Representative immunoblot shown of FLAG tagged CLMB wild type ($CLMB_{WT}$), S-acylation defective ($CLMB_{C7,14S}$) or myristoylation defective ($CLMB_{G2A}$), immunoprecipitated and detected using CLICK chemistry with biotin-azide followed by detection with IRdye 800CW streptavidin (n = 3 independent experiments). Asterisks indicate CLMB dimers formed due to absence of reducing agents (see methods).

**c** Representative immunoblot of acyl-PEG exchange performed on lysates expressing $CLMB_{WT}$-FLAG or lipidation mutants ($CLMB_{C7S}$, $CLMB_{C7,14S}$, $CLMB_{G2A}$). PEGylation events, a proxy for S-acylation, are indicated by asterisks. For each sample, input, cleaved ($NH_2OH$) and PEGylated (mPEG), and non-cleaved PEGylated conditions are shown. Cells were treated with 20 µM MG132 for 4 hours prior to harvesting. Endogenous, dually S-acylated calnexin is a positive control (n = 3 independent experiments).

**d** Pulse chase analysis of CLMB-FLAG S-acylation turnover using analogs of palmitate (17-ODYA) or methionine (L-AHA). Incorporation into immunoprecipitated CLMB-FLAG in the absence of analog (Neg Ctrl), or after 2 hours of analog treatment followed by 0 or 30 minutes without analog including DMSO (control) or palmostatin B. 17-ODYA or L-AHA were detected using CLICK with Cy5 and AZDye 488, respectively. A representative in-gel fluorescence scan is shown (n = 3 independent experiments).

**e** Data from (**d**) showing mean ± SEM of 17-ODYA signal normalized to L-AHA. Indicated p-values calculated by two-way ANOVA corrected by Tukey's multiple comparison test. N=3 independent experiments.

**f** Sub-cellular fractionation of lysates containing $CLMB_{WT}$-FLAG or lipidation mutants ($CLMB_{C7,14S}$, $CLMB_{G2A}$). Cells were treated with 20 µM MG132 for 4 hours prior to harvesting. Representative immunoblot showing input, cytoplasmic (cyto), and membrane (mem) fractions. GM130 and α-tubulin mark membrane and cytosolic fractions respectively.

**g** Data from (**f**) showing mean ± SEM cytoplasmic or membrane signals normalized to total (cytoplasmic + membrane signals). Indicated p-values calculated by two-way ANOVA corrected by Tukey's multiple comparison test. N= 3 independent experiments.

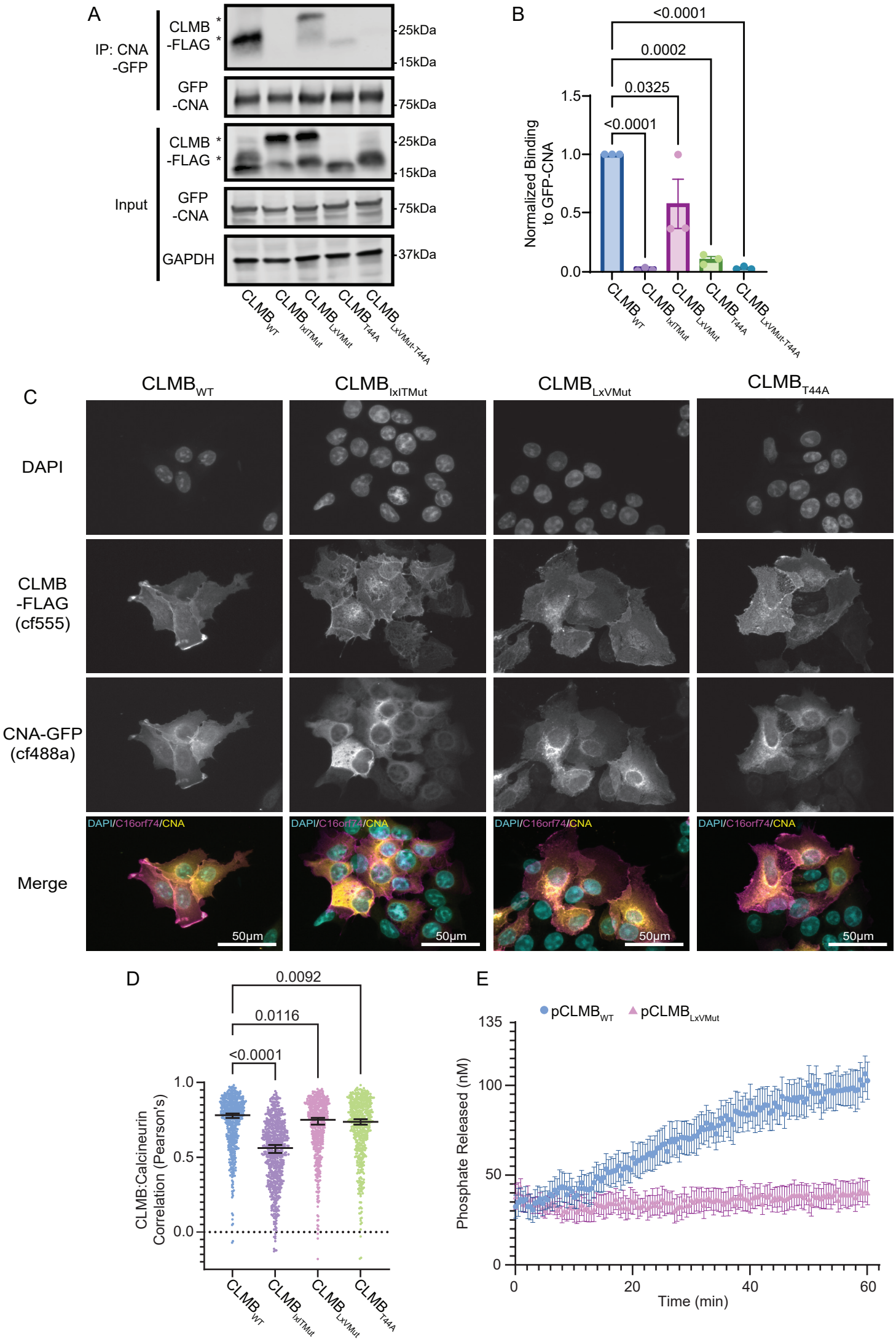
A
IP: CNA -GFP
CLMB -FLAG
GFP -CNA
Input
CLMB -FLAG
GFP -CNA
GAPDH
25kDa
15kDa
75kDa
37kDa
CLMB WT
CLMB IxITMut
CLMB LxVMut
CLMB T44A
CLMB LxVMut-T44A
B
<0.0001
0.0002
0.0325
<0.0001
Normalized Binding to GFP-CNA
1.5
1.0
0.5
0.0
C
CLMB WT
CLMB IxITMut
CLMB LxVMut
CLMB T44A
DAPI
CLMB -FLAG (cf555)
CNA-GFP (cf488a)
Merge
DAPI/C16orf74/CNA
50µm
D
0.0092
0.0116
<0.0001
CLMB:Calcineurin Correlation (Pearson's)
1.0
0.5
0.0
CLMB WT
CLMB IxITMut
CLMB LxVMut
CLMB T44A
E
pCLMB WT
pCLMB LxVMut
Phosphate Released (nM)
135
100
50
0
0
20
40
60
Time (min)

**Figure 2: Composite SLiM in calcimembrin mediates binding to and dephosphorylation by calcineurin.**

**a** Representative immunoblot of anti-GFP purification from lysates of HEK293 cells co-transfected with CNA-GFP and CLMB-FLAG ($CLMB_{WT}$, $CLMB_{IxITMut}$, $CLMB_{LxVMut}$, $CLMB_{T44A}$, or $CLMB_{LxVMut+T44A}$).

**b** Data from (**a**) showing mean ± SEM CLMB-FLAG pulled down normalized to CLMB-FLAG input levels and CNA-GFP pulled down. Indicated p-values calculated by two-way ANOVA corrected by Dunnett's multiple comparison test (n = 3 independent experiments).

**c** Representative immunofluorescence images of fixed MCF7 cells co-transfected with CLMB-FLAG ($CLMB_{WT}$, $CLMB_{IxITMut}$, $CLMB_{LxVMut}$, or $CLMB_{T44A}$) and CNA-GFP. CLMB was visualized using anti-FLAG, calcineurin with anti-GFP, and nuclei with Hoechst 33342. Scale bar = 50 µm.

**d** Data from (**c**) showing median with 95% CI Pearson's correlation coefficient of CLMB-calcineurin colocalization. Each point represents a single cell (n ≥ 500 for each condition). Indicated p-values calculated by Kruskal-Wallis with Dunn's multiple comparisons correction.

**e** Plot of phosphate released from 200 nM $pCLMB_{WT}$ (blue circles) or $pCLMB_{LxVMut}$ (pink squares) phospho-peptides dephosphorylated by 20 nM CNA/B and 1 µM CaM. Displayed is the mean ± SEM of phosphate released for ≥ 4 replicates at each timepoint.

A

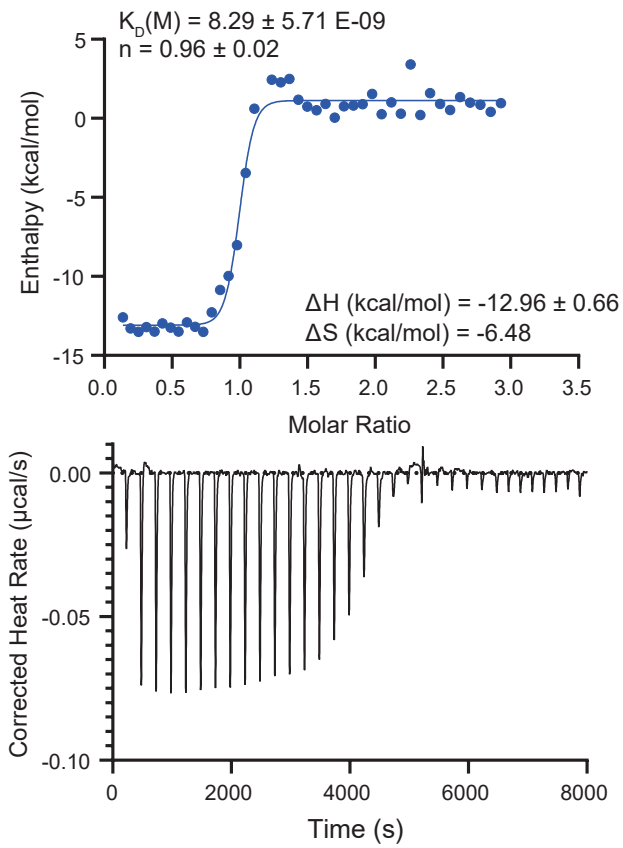


B

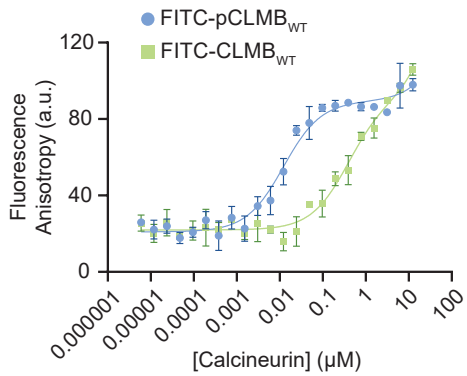


C

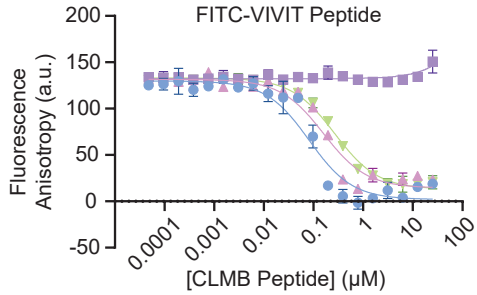


D

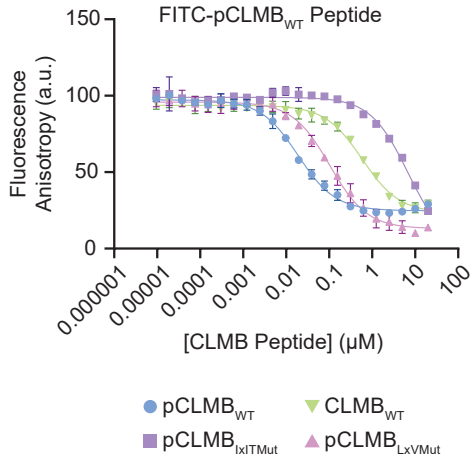


E

| Peptide Competitor | FITC-VIVIT | | FITC-pCLMB$_{WT}$ | |
|---|---|---|---|---|
| | $IC_{50}$(nM) | $K_i$(nM) | $IC_{50}$(nM) | $K_i$(nM) |
| pCLMB$_{WT}$ | 81.4 ± 16.2 | 80.9 ± 16.1 | 18.9 ± 1.2 | 13.4 ± 0.8 |
| pCLMB$_{IxITMut}$ | NA | NA | 6687 ± 878 | 4754 ± 624 |
| pCLMB$_{LxVMut}$ | 159 ± 30 | 158± 30 | 103 ± 9 | 73.2 ± 6.4 |
| CLMB$_{WT}$ | 267 ± 21 | 265 ± 21 | 585 ± 57 | 426 ± 40 |

**Figure 3: Phosphorylation and the LxVP motif contribute to PxIxIT binding.**

**a** Isothermal calorimetric enthalpy change displaying the thermometric evaluation of the affinity between CNA/B complex and unlabeled pWT peptide (top), and binding isotherm obtained by titration of unlabeled pWT into CNA/B complex (40 μM) (bottom). A dissociation constant ($K_D$) = 8.3 ± 5.7 nM was obtained.

**b** Fluorescence polarization (FP) saturation binding curves of two different FITC-labeled peptide tracers (5nM), FITC-pCLMB$_{WT}$ and FITC-CLMB$_{WT}$ were incubated with serial dilutions of CNA/B (0 to 12.5μM). The FP values were recorded at room temperature after a 30 minute incubation time. FP data were fitted to a one-site binding model (mean ± s.d., n = 2 independent experiments) using GraphPad Prism 10.0.

**c** Competitive binding assay of unlabeled pCLMB$_{WT}$, CLMB$_{WT}$, pCLMB$_{IxITMut}$, and pCLMB$_{LxVMut}$ peptides. The unlabeled peptides were titrated against a constant concentration of FP probe (FITC-PVIVIT peptide, 5 nM) in the presence of 2 μM CNA/B. Data (mean ± s.d., n = 2 independent experiments) were analyzed in GraphPad Prism 10.0.

**d** Competitive binding assay of unlabeled pCLMB$_{WT}$, CLMB$_{WT}$, pCLMB$_{IxITMut}$, and pCLMB$_{LxVMut}$ peptides. The peptides were titrated against a constant concentration of FP probe (FITC-pCLMB$_{WT}$ peptide, 5 nM) in the presence of 0.08 μM CNA/B . Data (mean ± s.d., n = 2 independent experiments) were analyzed in GraphPad Prism 10.0.

**e** Table displaying the experimentally obtained $IC_{50}$ values and converted $K_i$ values resulting from the competitive binding assay of unlabeled pCLMB$_{WT}$, CLMB$_{WT}$, pCLMB$_{IxITMut}$, and pCLMB$_{LxVMut}$ peptides. The unlabeled peptides were titrated against a constant concentration of FP probe (FITC-pCLMB$_{WT}$ or FITC-PVIVIT, 5 nM) in the presence of 0.08 μM and 2μM CNA/B, respectively. Data (mean ± s.d., n = 2 independent experiments) were analyzed in GraphPad Prism 10.0.

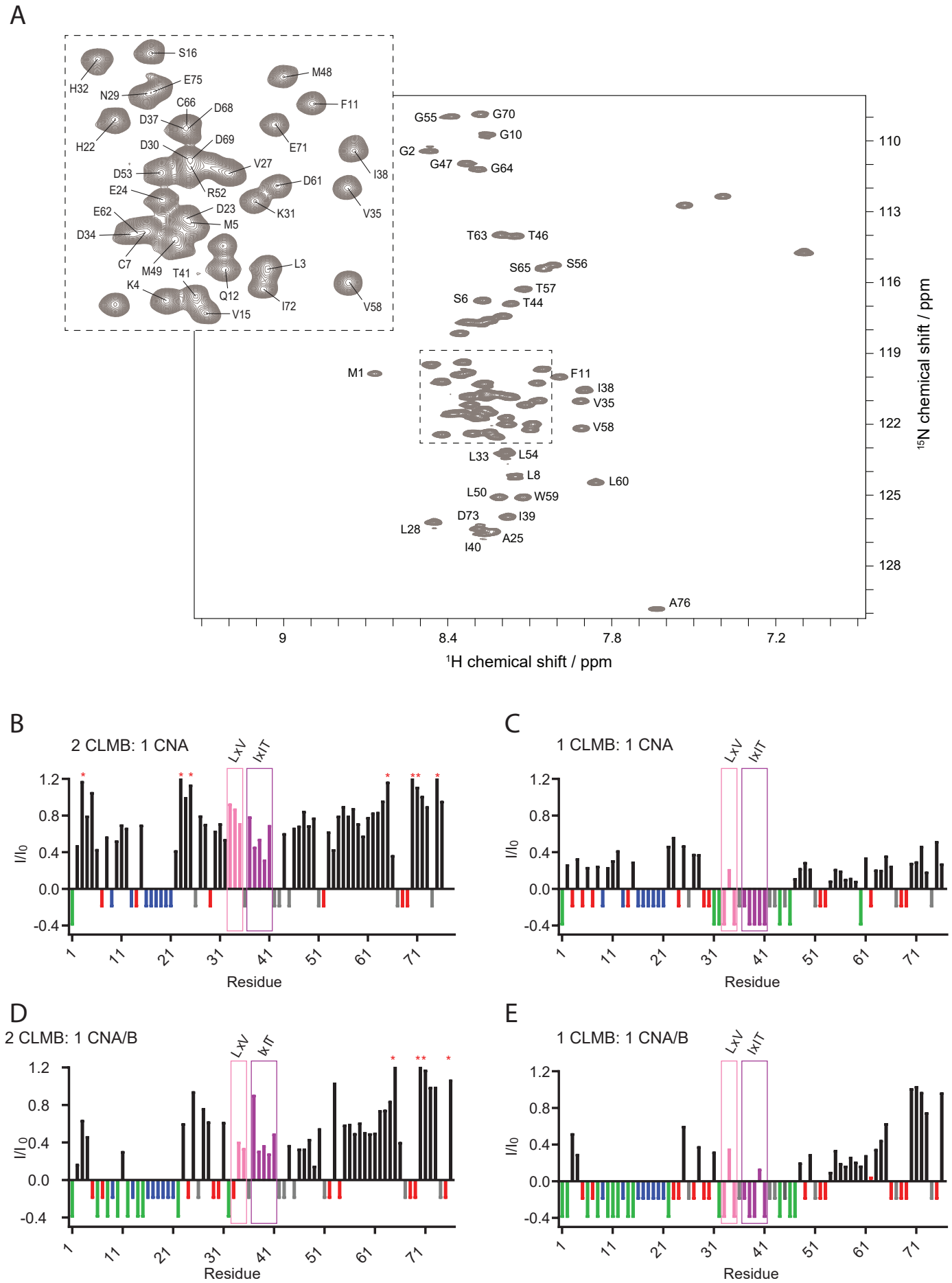
A
S16
H32
E75
N29
M48
F11
C66
D68
D37
H22
D30
D69
E71
D53
V27
I38
E24
R52
D61
E62
D23
K31
V35
D34
M5
C7
M49
T41
L3
K4
Q12
I72
V58
V15
G55
G70
G10
G2
G47
G64
T63
T46
S65
S56
T57
S6
T44
M1
F11
I38
V35
V58
L33
L54
L8
L60
L50
W59
D73
I39
L28
A25
I40
A76
110
113
116
119
122
125
128
9
8.4
7.8
7.2
$^{1}$H chemical shift / ppm
$^{15}$N chemical shift / ppm
B
2 CLMB: 1 CNA
LxV
IxIT
I/I0
Residue
C
1 CLMB: 1 CNA
LxV
IxIT
I/I0
Residue
D
2 CLMB: 1 CNA/B
LxV
IxIT
I/I0
Residue
E
1 CLMB: 1 CNA/B
LxV
IxIT
I/I0
Residue

**Figure 4**: **CLMB-CN binding extends beyond the LxVP and PxIxIT motifs.**

**a** $^{15}N$ HSQC spectra of free CLMB with the resonance assignment (red).

**b** NMR spectral analysis of the interaction of CLMB with CNA at 2:1 (CLMB: CNA); **c** with CNA at 1:1 (CLMB: CNA); **d** with CNA/B complex at 2:1 (CLMB: CNA/B); **e** with CNA/B at 1:1 (CLMB: CNA/B). The graphs display the intensity ratios of the CLMB resonances with and without the titrant (CNA or CNA/B) at different molar ratios. The ratios corresponding to the LxV motif, represented in pink, and IxIT motif, in purple. Residues where we cannot access the intensity ratio are represented with negative numbers. Peaks resulting in complete broadening are shown as negative bars in green ($I/I_0 = -0.4$). Residues that were not assigned in the apo CLMB are shown in blue ($I/I_0 = -0.2$), prolines that are not represented in a $^{15}N$-HSQC are shown in grey ($I/I_0 = -0.2$), and residues where we cannot unambiguously assign the bound resonance is shown in red, ($I/I_0 = -0.2$). Residues that have an overlap in the resonance and hence when one of the resonances broadens results in $I/I_0$ higher than 1 is marked with a * sign.

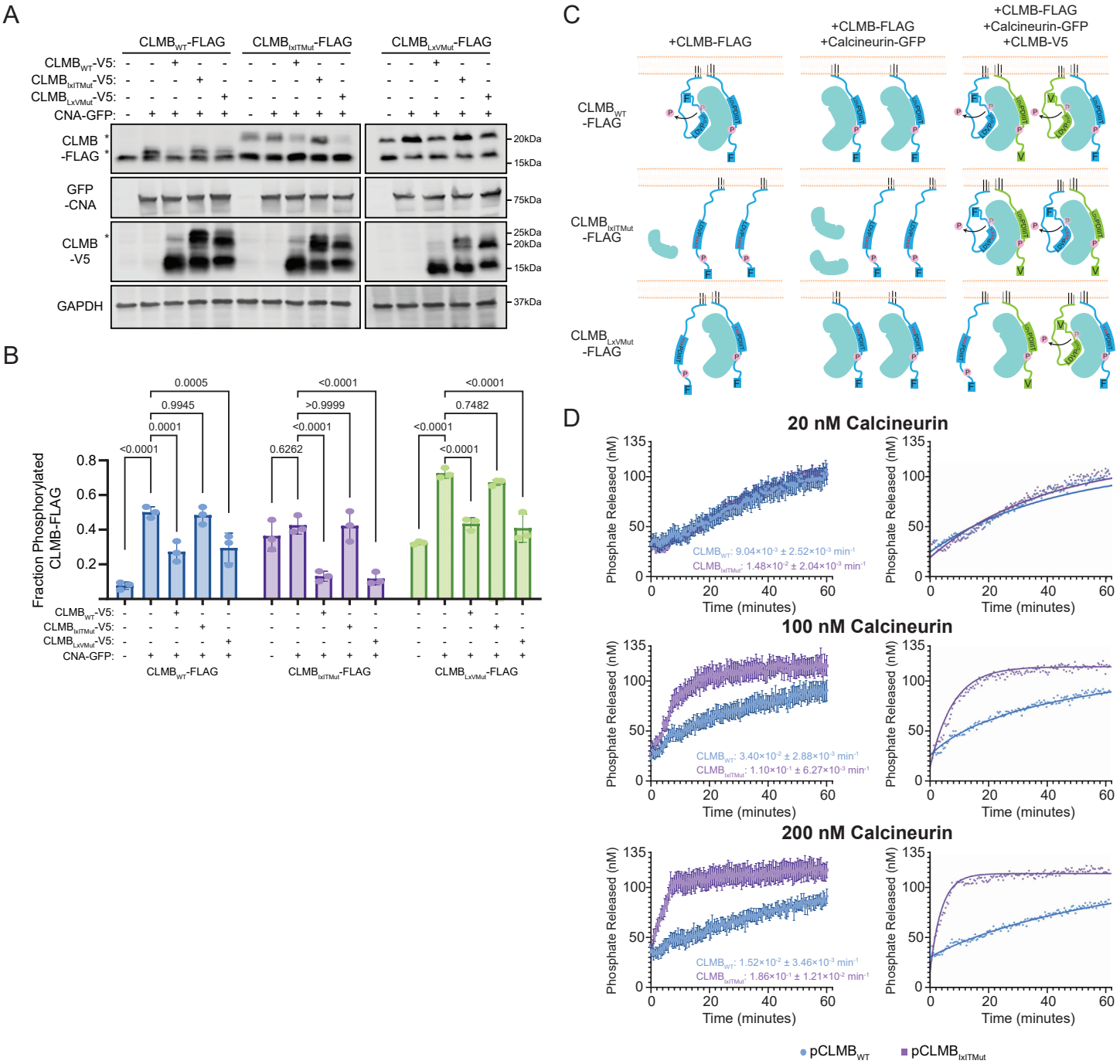
A
CLMB$_{WT}$-FLAG
CLMB$_{IxITMut}$-FLAG
CLMB$_{LxVMut}$-FLAG
CLMB$_{WT}$-V5:
CLMB$_{IxITMut}$-V5:
CLMB$_{LxVMut}$-V5:
CNA-GFP:
CLMB -FLAG
GFP -CNA
CLMB -V5
GAPDH
20kDa
15kDa
75kDa
25kDa
20kDa
15kDa
37kDa
B
Fraction Phosphorylated CLMB-FLAG
0.8
0.6
0.4
0.2
0.0005
0.9945
0.0001
<0.0001
<0.0001
>0.9999
<0.0001
0.6262
<0.0001
0.7482
<0.0001
<0.0001
CLMB$_{WT}$-FLAG
CLMB$_{IxITMut}$-FLAG
CLMB$_{LxVMut}$-FLAG
C
+CLMB-FLAG
+CLMB-FLAG +Calcineurin-GFP
+CLMB-FLAG +Calcineurin-GFP +CLMB-V5
CLMB$_{WT}$ -FLAG
CLMB$_{IxITMut}$ -FLAG
CLMB$_{LxVMut}$ -FLAG
D
20 nM Calcineurin
100 nM Calcineurin
200 nM Calcineurin
Phosphate Released (nM)
Time (minutes)
CLMB$_{WT}$: 9.04×10$^{-3}$ ± 2.52×10$^{-3}$ min$^{-1}$
CLMB$_{IxITMut}$: 1.48×10$^{-2}$ ± 2.04×10$^{-3}$ min$^{-1}$
CLMB$_{WT}$: 3.40×10$^{-2}$ ± 2.88×10$^{-3}$ min$^{-1}$
CLMB$_{IxITMut}$: 1.10×10$^{-1}$ ± 6.27×10$^{-3}$ min$^{-1}$
CLMB$_{WT}$: 1.52×10$^{-2}$ ± 3.46×10$^{-3}$ min$^{-1}$
CLMB$_{IxITMut}$: 1.86×10$^{-1}$ ± 1.21×10$^{-2}$ min$^{-1}$
pCLMB$_{WT}$
pCLMB$_{IxITMut}$

**Figure 5: Calcineurin dephosphorylates calcimembrin by forming multimers.**

**a** Representative immunoblot of CLMB-FLAG phosphorylation-induced mobility shifts induced by calcineurin overexpression. Performed using lysates from Flp-In-T-REx HEK cells inducibly expressing $CLMB_{WT}$-FLAG, $CLMB_{IxITMut}$-FLAG, or $CLMB_{LxVMut}$-FLAG and transfected with empty vector, CNA-GFP, or CNA-GFP with CLMB-V5 ($CLMB_{WT}$, $CLMB_{IxITMut}$, $CLMB_{LxVMut}$). Asterisks indicate phosphorylated CLMB.

**b** Data from (**a**) showing mean ± SEM phospho-CLMB-FLAG normalized to total CLMB-FLAG. Displayed p-values calculated by two-way ANOVA corrected by Dunnett's multiple comparison test (n = 3 independent experiments).

**c** Cartoon representation of calcineurin-CLMB complex formation and CLMB dephosphorylation under the conditions used in (**a**), i.e. CLMB-FLAG (blue) overexpression, CLMB-FLAG (blue with "F") and calcineurin overexpression, or CLMB-FLAG, calcineurin, and CLMB-V5 (green with "V") overexpression. Cartoons depict complexes formed by $CLMB_{WT}$-FLAG, $CLMB_{IxITMut}$-FLAG, and $CLMB_{LxVMut}$-FLAG with red X's to indicate motif mutation. Black arrows depict CLMB dephosphorylation.

**d** (Right) Plots of phosphate released from 100 nM $pCLMB_{WT}$ (blue circles) or $pCLMB_{IxITMut}$ (purple squares) phosphopeptide dephosphorylated by 20 nM (left), 100 nM (middle) or 200 nM (right) CNA/B and 1 μM calmodulin. Displayed is the mean ± SEM of phosphate released for ≥ 5 replicates at each timepoint. (Left) Plots fit by simulation to the model shown in S5A and S5B using Kintek Explorer.

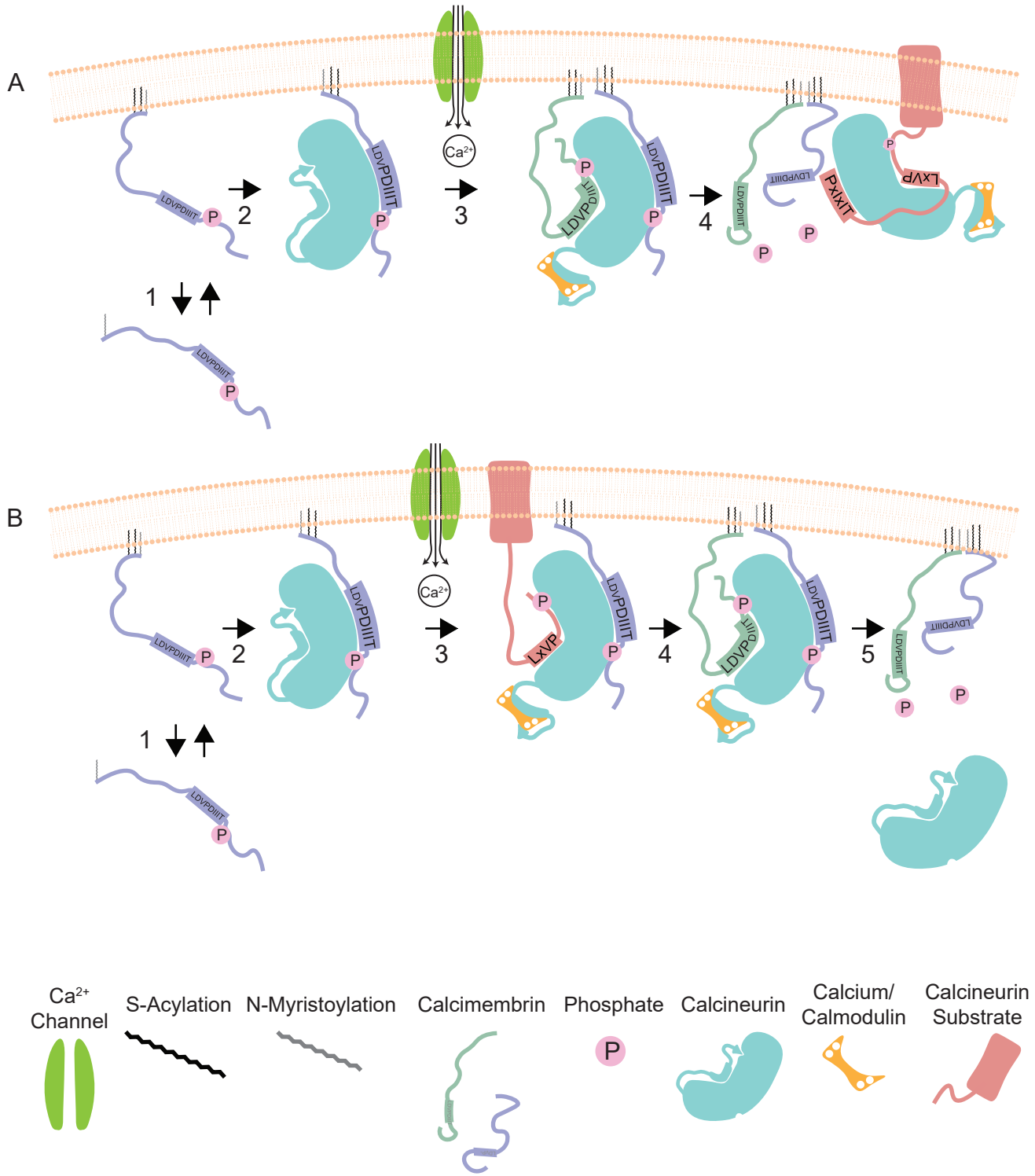
A
B
1
2
3
4
5
Ca2+
LDVPDIIIT
P
LXVP
PxIxIT
Ca2+ Channel
S-Acylation
N-Myristoylation
Calcimembrin
Phosphate
Calcineurin
Calcium/ Calmodulin
Calcineurin Substrate

**Figure 6: A model for how calcimembrin modulates calcineurin signaling.**

**a** (1) CLMB is dynamically acylated and localizes to membranes where it (2) recruits CN. When CLMB levels are low, calcineurin remains tightly bound to phosphorylated CLMB regardless of $Ca^{2+}$ signals. (3) As CLMB levels rise, $Ca^{2+}$ and CaM binding allow calcineurin-CLMB multimers to form and CLMB to be dephosphorylated. (4) Calcineurin is then freed to engage and dephosphorylate nearby substrates.

**b** (1) CLMB is dynamically acylated and localizes to membranes where it (2) recruits calcineurin. When CLMB levels are low, calcineurin remains tightly bound to phosphorylated CLMB. (3) $Ca^{2+}$ and CaM activate calcineurin, allowing CLMB to present it to nearby substrates for LxVP-mediated binding and dephosphorylation. (4) When CLMB accumulates at membranes, calcineurin-CLMB multimers form, and (5) dephosphorylation triggers calcineurin release to terminate signaling.